Low Temperature Synthesis of Insertion Oxides for Lithium Batteries

A. Manthiram* and J. Kim

Texas Materials Institute, ETC 9.104, The University of Texas at Austin, Austin, Texas 78712

Received April 2, 1998. Revised Manuscript Received June 30, 1998

The increasing demand for portable electronic devices has created significant activity in the development of compact lightweight batteries of high-energy density, and lithium batteries have become attractive in this regard. The commercial lithium cells use lithium cobalt oxide cathodes and the high cost and toxicity of cobalt has prompted the design and synthesis of alternate insertion hosts. Several low-temperature synthesis routes have been pursued during the past few years both to improve the properties of known oxide hosts as well as to access new insertion oxides, particularly metastable phases. This review, after providing a brief background to lithium batteries, lithium insertion compounds, and lithium ion batteries, presents the low-temperature synthesis and electrochemical properties of manganese, cobalt, nickel, iron, vanadium, chromium, titanium, molybdenum, and tin oxides. The use of soft chemistry methods such as sol−gel processing, ion-exchange reactions, hydrothermal reactions, and oxidation−reduction reactions in solutions to obtain oxide hosts are presented.

Contents

Introduction

Rapid technological developments and the miniaturization in electronics have created an ever increasing demand for lightweight, compact batteries.[1] For example, popular portable electronic devices such as laptop computers, camcorders, and cellular phones require small, but efficient and reliable batteries. In addition, there is enormous interest in developing advanced, high-energy-density batteries for electric vehicle propulsion.[2]

The development of high-energy-density batteries requires the use of high-capacity electrode materials that can also offer high cell voltages V_c. A high V_c can be achieved with negative (anode) and positive (cathode) electrodes that have, respectively, smaller and larger work functions ϕ_a and ϕ_c. Considering only the electron transfer between the two electrodes, a schematic energy diagram at open circuit is illustrated in Figure 1 and the open-circuit voltage V_{oc} of the cell is given as

$$V_{oc} = (\phi_c - \phi_a)/e \quad (1)$$

where e is the electronic charge.[3] Thermodynamic stability considerations also necessitate the Fermi energies E_F of the cathodes and anodes to lie within the band gap E_g of the electrolyte, as shown in Figure 1, so that no unwanted reduction or oxidation of the electrolyte occurs.

Lithium metal having a high specific capacity, and standard oxidation potential (smaller work function ϕ_a) became an obvious choice for the anode in the development of high-energy-density batteries. Lithium batteries consisting of a lithium anode and a lithium insertion compound $Li_xM_yX_z$ (M = transition metal and X = nonmetal), with a larger work function ϕ_c for M^{n+} as the cathode, can offer high cell voltages (eq 1). However, eq 1 considers only the electron transfer, and the energy effects associated with the Li^+ transfer can also influence V_{oc}. Therefore, V_{oc} of a lithium cell will more appropriately be related to the difference of the lithium chemical potential between the cathode ($\mu_{Li(c)}$) and anode ($\mu_{Li(a)}$):[4]

$$V_{oc} = (\mu_{Li(c)} - \mu_{Li(a)})/ne \quad (2)$$

where n and e are, respectively, the number of electrons transferred and electronic charge. Lithium batteries offer several advantages, such as higher voltages, higher energy density, and longer shelf life compared to other systems. Figure 2 compares the gravimetric and volu-

* Corresponding author. Phone: (512)471-1791. Fax: (512)471-7681. E-mail: rmanth@mail.utexas.edu.

10.1021/cm980241u CCC: $15.00
Published on Web 09/18/1998

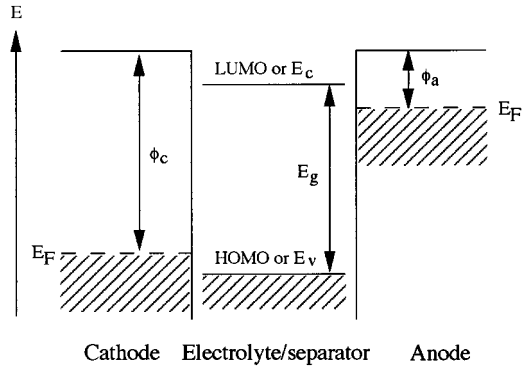

Figure 1. Schematic energy diagram of a cell at open circuit.

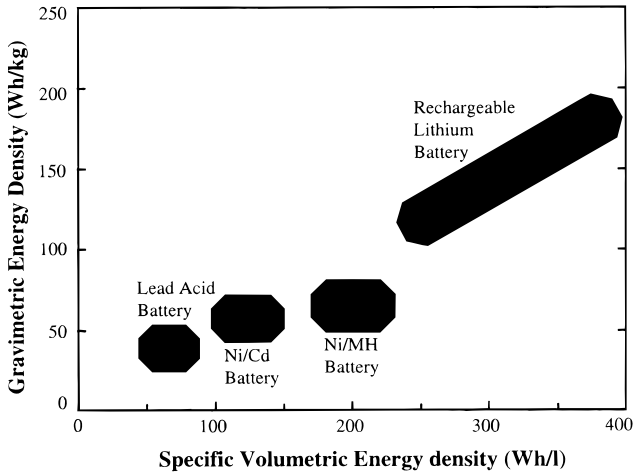

Figure 2. Comparison of the gravimetric and volumetric energy densities of rechargeable lithium batteries with those of other systems (adapted from ref 5).

metric energy densities of various rechargeable systems,[5] and it is clear that lithium batteries are lighter in weight and smaller in dimension than other systems. In addition, the use of nonaqueous electrolytes in lithium batteries permits the operation over a wide range of temperatures.

Lithium Insertion Compounds

The advantages of lithium batteries prompted solid-state chemists in the 1970s to develop lithium insertion compounds. Intensive research during the past 25 years has led to the identification of several lithium insertion compounds as cathodes.[6−9] The electrochemical potential ranges of some lithium insertion compounds versus metallic lithium are given in Figure 3. A lithium insertion compound consists of a host matrix into/from which the guest species Li^+ can be reversibly inserted/extracted during the discharge/charge process. The lithium insertion compound should have the following properties to be successful as an electrode host in lithium cells:

1. The transition metal ion in the insertion compound cathode $Li_xM_yX_z$ should have a larger work function ϕ_c for M^{n+} to maximize the cell voltage (eq 1). On the other hand, if the insertion compound $Li_xM_yX_z$ is to be used as an anode, then the M^{n+} ion should have a smaller work function ϕ_a to maximize cell voltage. The change in cell voltage, $\Delta(\phi_c - \phi_a)/e$ or more appropriately $\Delta(\mu_{Li(c)} - \mu_{Li(a)})/ne$, during the lithium insertion/extraction (discharge/charge) process should be small so that the operating cell voltage does not vary significantly.

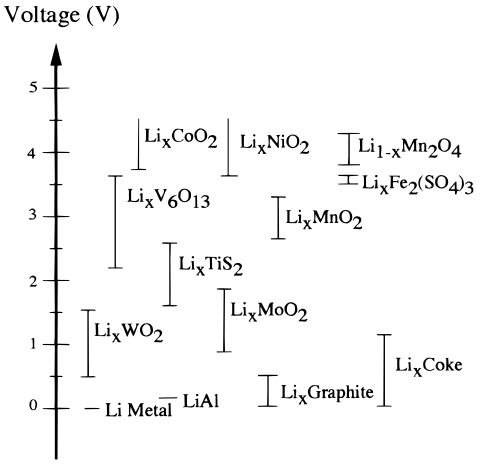

Figure 3. Electrochemical potential ranges of some lithium insertion compounds in reference to metallic lithium.

2. The insertion compound $Li_xM_yX_z$ should allow an insertion/extraction of a large amount of lithium x to maximize the cell capacity. A high cell capacity together with a high cell voltage can maximize the energy density.

3. The lithium insertion/extraction process should be reversible with no or minimal changes in the host structure over the entire range x of lithium insertion/extraction.

4. The insertion compound should support good electronic (σ_e) and Li^+ ion (σ_{Li}) conductivities to minimize cell polarizations. The high conductivities are essential to support a large current density and hence to provide a high power density.

5. The insertion compound should be chemically stable over the entire voltage range without undergoing any reaction with the electrolyte.

6. From a commercial point of view, the insertion compound should be inexpensive, environmentally friendly, and lightweight to minimize the battery weight.

Although transition metal sulfides were initially pursued as cathode hosts, it is difficult to achieve higher cell voltages with sulfides.[10] An overlap of the higher valent M^{n+}-d energies with the top of the S-3p energy and the formation of S_2^{2-} ions lead to an inaccessibility of higher oxidation states for M^{n+} in sulfides. Stabilization of higher oxidation states in lithium insertion compounds $Li_xM_yX_z$ is essential to maximize ϕ_c and achieve higher cell voltages. On the other hand, the location of the O-2p energy much below the S-3p energy makes the higher valent states accessible in transition metal oxides. Consequently, transition metal oxide hosts provide the highest cell voltages of ∼4 V, while still keeping the Fermi energies E_F of the cathode and anode within the band gap of the nonaqueous electrolytes used in lithium cells (Figure 1).

Among the known lithium insertion compounds (Figure 3), the layered $LiMO_2$ (M = Co and Ni) and the spinel $Li[Mn_2]O_4$ have become attractive cathodes because they offer a cell voltage of ∼4 V versus a metallic lithium anode.[11,12] The higher voltage originates from a larger work function ϕ_c associated with the highly oxidized $Co^{3+/4+}$, $Ni^{3+/4+}$, and $Mn^{3+/4+}$ couples in an oxide. The $LiMO_2$ oxides for M = V, Cr, Co, and Ni have

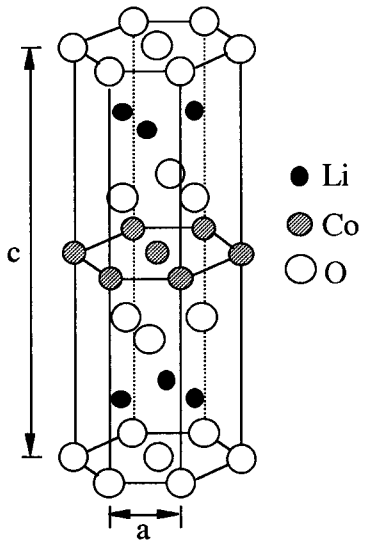

Figure 4. The layer structure of $LiCoO_2$.

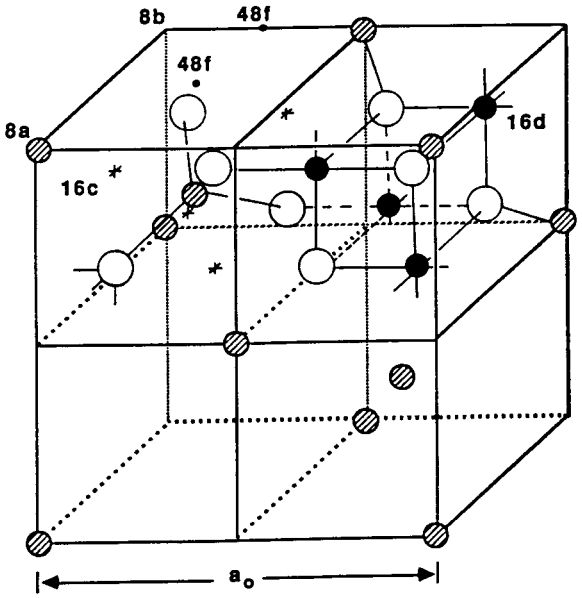

Figure 5. The crystal structure of spinel. Hatched, solid and open circles refer, respectively, to Li^+, $Mn^{3+/4+}$, and O^{2-} ions in $LiMn_2O_4$ spinel. The numbers refer to the various crystallographic positions in the spinel structure.

a layer structure isostructural with α-$NaFeO_2$.[13] In $LiMO_2$, the Li^+ and M^{3+} ions occupy alternate (111) planes of a rock salt structure as shown in Figure 4. A 2-dimensional motion of the Li^+ ions between the strongly bonded MO_2 layers provides a high σ_{Li}. The $LiMO_2$ oxides have diffusion coefficients of $10^{-7}-10^{-9}$ cm^2/s for Li^+ ions, depending on the technique used.[14]

On the other hand, the spinel $Li[Mn_2]O_4$ oxide has a 3-dimensional structure in which the Li^+ ions and the $Mn^{3+/4+}$ ions occupy, respectively, the 8a tetrahedral and 16d octahedral sites of the cubic close-packed oxygen array as shown in Figure 5. A strong edge-shared octahedral $[Mn_2]O_4$ array permits a reversible extraction of the Li^+ ions without collapsing the spinel framework.[12] However, the 3-dimensional spinel lattice leads to a slightly slower Li^+ ion diffusion compared with the layered $LiMO_2$ structure.

Another 3-dimensional host $Fe_2(SO_4)_3$, with a NASICON-related framework structure, also offers a flat voltage of 3.6 V versus metallic Li.[15] Although the Fe-containing cathodes may be attractive from both cost and toxicity points of view, $Fe_2(SO_4)_3$ suffers from a low σ_e due to the presence of Fe−O−S−O−Fe linkages rather than the desired direct Fe−Fe or Fe−O−Fe linkages. In contrast, both the layered $LiMO_2$ and the spinel $Li[M_2]O_4$ provide good σ_e arising from a direct M−M and M−O−M linkages in the edge-shared octahedral arrangement.

Lithium Ion Batteries

Despite a successful development of several lithium insertion compounds, the commercialization of rechargeable lithium batteries was delayed until the 1990s due to the difficulties posed by metallic lithium anodes. The chemical reactivity of metallic lithium anode with the nonaqueous electrolytes used in lithium cells creates a passivating film on the anode. Although the passivating film helps to prevent further corrosion, it leads to a nonuniform lithium plating during charging, which results not only in a total cell failure due to dendritic short circuiting, but also in serious safety problems[16] due to local over heating. Several strategies such as the use of a lithium alloy instead of pure lithium anode and attempts to identify nonreactive electrolytes have failed to solve this problem. Other approaches, such as (1) achieving controlled and optimized surface films by adding other agents (such as CO_2 or HF) to electrolytes,[17] and (2) use of solid polymer electrolytes consisting of a lithium salt in a ploymer matrix instead of liquid electrolytes, are currently being pursued. However, the lower conductivity of polymer electrolytes poses a problem to operate them at ambient temperatures and the long-term stability of polymer batteries remains to be established. In addition, polymer batteries require cathodes with lower voltages (3 V) to maintain a stable interface between the electrode and electrolyte.

The difficulties of metallic lithium anode with liquid electrolytes have ultimately forced the use of lithium insertion compounds as both anodes and cathodes.[18] Cells employing insertion compounds as cathodes and anodes are called "lithium-ion" or "rocking-chair" cells because the lithium ions shuttle or rock between the cathode and anode hosts during the discharge−charge cycles, as illustrated in Figure 6.[14] In the lithium-ion cell shown in Figure 6, the Li^+ ions are extracted from the layered $LiCoO_2$ cathode and inserted into the carbon anode during charge while the electrons flow through the external circuit from the cathode to anode. The direction of flow of Li^+ ions and electrons is reversed during discharge. Lithium-ion cells, however, require a careful selection of electrode pairs so as to maintain an acceptable cell voltage of >2 V over the discharge cycle and to minimize the added weight associated with the host framework of an insertion compound anode. The lightweight carbon Li_xC_6, with a discharge voltage of 0−1 V, versus metallic lithium (Figure 3) has become an attractive anode host for lithium-ion cells.[18,19] On the other hand, the layered $LiMO_2$ (M = Co and Ni) and the spinel $Li[Mn_2]O_4$ with a discharge voltage around 4 V versus metallic lithium have become attractive cathode hosts for lithium-ion cells.

There are, however, a few issues with the $LiMO_2$ (M = Co and Ni) and $Li[Mn_2]O_4$ cathodes and the carbon

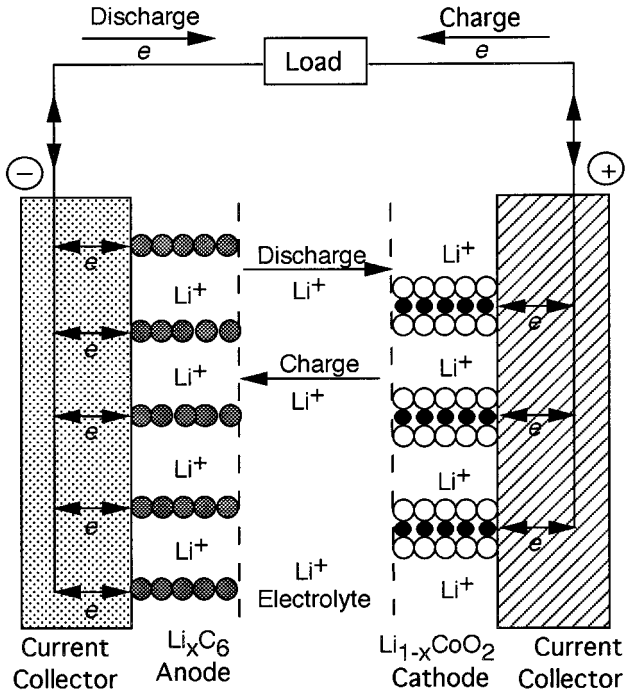

Figure 6. Schematic illustration of the discharge and charge processes in a rechargeable lithium ion battery. In the Li_x-CoO_2 cathode, the solid and open circles refer, respectively, to Co and O atoms (adapted from ref 14).

anodes that need attention. An oxidative decomposition of most of the electrolytes above ~4.3 V as well as cathode degradation arising from, for example, lithium ordering and structural distortions around $x \approx 0.5$, limit the use of $Li_{1-x}MO_2$ (M = Co and Ni) to $x < 0.5$ and thereby lower the utilizable capacity to <150 mAh/g.[20] Also, cobalt and nickel are expensive and toxic. In addition, the reversibility of lithium insertion/extraction in $LiMO_2$ and hence the cell performance are influenced strongly by the ordering of Li^+ and M^{3+} ions in the lattice.[21,22] Although $LiCoO_2$ can be readily obtained as an ordered material, $LiNiO_2$ is difficult to obtain as an ordered, stoichiometric material because nickel tends to form Ni^{2+}.[23,24] The cost and environmental concerns of cobalt and nickel make the spinel $Li[Mn_2]O_4$ more attractive because manganese is inexpensive and environmentally benign. But the Jahn−Teller distortion associated with the Mn^{3+} ions causes capacity fading upon cycling, and also limits the utilizable capacity to <120 mAh/g, corresponding to a lithium extraction/insertion of 0.4 Li per Mn. On the other hand, the carbon anode exhibits an initial loss in capacity probably due to side processes involving decomposition of the electrolyte.

The commercially available lithium-ion cells are made with carbon anodes and the more expensive and toxic $LiCoO_2$ cathodes. There is enormous interest, primarily driven by cost and environmental concerns, either to improve the performance of manganese oxide cathodes by innovative synthesis and processing procedures or to develop new low-cost cathodes. There is an interest to identify new anode hosts as well. This review focuses on the low-temperature "soft chemistry" synthesis procedures employed in recent years both to develop new oxide electrodes and to overcome the difficulties of the known electrode hosts. For a more comprehensive review of other aspects, the readers may refer to other review papers.[6−9,25]

Low-Temperature Synthesis

Transition metal oxides are traditionally made by repeated grinding and firing at elevated temperatures of the solid reactants to overcome the diffusional limitations. Such a high-temperature approach generally gives the thermodynamically more stable phases and often results in an inaccessibility of metastable phases and unusual valence states. This difficulty has prompted solid-state chemists to design and develop "soft chemistry" synthesis routes that can lower the processing temperatures.[26] Low-temperature methods such as sol−gel processing, design of molecular precursors, coprecipitation, chemical and electrochemical lithium insertion/extraction, electrochemical oxygen insertion, molten flux reactions, ion-exchange reactions, and hydrothermal methods have attracted much attention in recent years.[26−29] An intimate or atomic-scale mixing of the components or the availability of the structural framework in these methods lowers the processing temperatures ($T < 700$ °C) and provides kinetic accessibility to metastable phases and unusual valence states. In addition, the low-temperature methods can offer products with smaller particle size, which may be beneficial for some applications.

We present in this review the use of low-temperature methods in developing electrode hosts for lithium batteries. Specifically, synthesis involving sol−gel process, ion-exchange reactions, hydrothermal methods, reduction of oxo ions, and oxidation of aquo ions are discussed. The recent developments in the low-temperature synthesis and electrochemical properties of manganese, cobalt, nickel, iron, vanadium, chromium, titanium, molybdenum, and tin oxides are presented. The smaller particle size offered by the low-temperature approach may be particularly attractive to achieve faster lithium ion diffusion and hence higher power density in lithium cells.

Manganese Oxides

The versatile use of manganese oxides in primary cells, due to its low cost and nontoxic nature, has stimulated an intensive investigation of manganese oxide cathodes for rechargeable lithium cells. Efforts both to improve the performance of spinel manganese oxides and to develop new manganese oxide hosts have been made by low-temperature procedures and the results are presented below.

Sol−Gel Synthesis. Sol−gel procedures involving the reaction between manganese (II) acetate and LiOH or Li_2CO_3 in aqueous solutions[30−32] and propionic acid[33] have been pursued to obtain $Li_xMn_2O_4$ spinel oxides. More recently, the Pechini process involving lithium and manganese nitrates, citric acid, and ethylene glycol to give a polymeric precursor followed by firing has also been utilized to obtain spinel oxides.[34] These solution-based procedures yield spinel phases at temperatures as low as 300 °C, with particle size in the submicron range. The samples obtained by the low-temperature procedures have been found to have lithium chemical

diffusion coefficient of at least an order of magnitude higher than that observed for samples obtained by high-temperature procedures.[31] The enhancement in diffusion has been attributed to defects, microstructure, and compositional inhomogeneities at the grain boundaries. The higher diffusion rate may be particularly attractive to achieve higher power densities with spinel cathodes. The solution-based procedures give better electrochemical performance in the 4 V region compared with the conventional solid-state methods. A capacity of ~134 mA h g^{-1} has been achieved in the 4 V region for the samples obtained by the Pechini process.[34] In many cases, a moderate firing temperature of 600 °C gives optimum electrochemical performance.

Ion-Exchange Reactions. Both the success of layered $LiCoO_2$ cathodes in commercial lithium-ion cells and the faster lithium ion diffusion in layered structures have created concerted efforts to develop layered manganese oxide cathodes. Although several $LiMO_2$ (M = V, Cr, Co, and Ni) oxides obtained by the conventional high-temperature procedures adopt the layer structure shown in Figure 4, $LiMnO_2$ does not. The Jahn−Teller distortion associated with Mn^{3+} leads to an orthorhombic rock salt structure in which the oxygen array is distorted from the ideal cubic close packing. The structure consists of corrugated layers of the MnO_6 and LiO_6 octahedra that are not parallel to the close-packed oxygen layers. α-$NaMnO_2$, on the other hand, is isostructural with $LiCoO_2$. Accordingly, ion-exchange reactions with α-$NaMnO_2$ have been pursued to obtain layered $LiMnO_2$. Although ion-exchange reactions with molten LiCl, LiBr, or LiI at 460−650 °C give the lithiated spinel $Li_2Mn_2O_4$ and orthorhombic $LiMnO_2$,[35] those with LiCl or LiBr in hexanol[36] or methanol[37] at lower temperatures (T < 150 °C) give the layered $LiMnO_2$. Electrochemical studies together with X-ray diffraction data,[38] however, reveal that the layered $Li_{1-y}MnO_2$ transforms irreversibly to the spinel $Li_xMn_2O_4$ upon electrochemical cycling due to a migration of the Mn atoms from the Mn layers to the lithium layers. Thus the spinel lattice is more stable than the layered lattice for the Li−Mn−O oxides and the metastable, layered $LiMnO_2$ has a stability problem.

Ion-exchange reactions of γ-MnOOH with LiOH have also been pursued.[39] These reactions yield orthorhombic $LiMnO_2$ that are less crystalline than that obtained by solid-state reactions and are referred to as low-temperature $LiMnO_2$. Whereas γ-MnOOH has a hexagonal close packing of oxygen atoms, $LiMnO_2$ has a cubic close packing of oxygen atoms. Thus, the reaction involves a significant amount of local rearrangement rather than a simple ion exchange. Although the low-temperature $LiMnO_2$ shows high capacity (210 mA h g^{-1} at 4.3−2.5 V) initially due to smaller particle size and higher surface area, it too transforms to a spinel-like phase upon electrochemical cycling like the layered $LiMnO_2$. The formation of a spinel-like phase is indicated by an increase in capacity in the 4 V region and a decrease in capacity in the 3 V region upon cycling.

The tendency of the Li−Mn−O oxides to transform to the spinel-like phases upon electrochemical cycling and the problems associated with the Jahn−Teller distortion in the spinel lattice have created interest in identifying other A−Mn−O oxides with nonclose-packed structures. In this regard, $Na_{0.44}MnO_2$, consisting of columns of edge-shared square pyramids and sheets of edge-shared octahedra of two and three units in width has been investigated.[40] The Na^+ ions occupying the tunnels in the resulting structure have been partially ion exchanged with Li^+ using $LiCF_3SO_3$ or $LiN(CF_3SO_2)_2$ to give $Na_{0.14}Li_{0.3}MnO_2$. Evaluation of $Na_{0.14}Li_{0.3}MnO_2$ in lithium polymer cells at 85 °C reveals that a capacity of ~140 mA h g^{-1} can be achieved in the voltage range 3.8−1.8 V at low current densities without transforming to the spinel-like phase.

Acid Digestion Reactions. Acid treatment of the $LiMn_2O_4$ spinel at ambient temperature is known to give λ-MnO_2, with the $[Mn_2]O_4$ spinel framework, by a disproportionation of Mn^{3+} into Mn^{4+} (in solid) and Mn^{2+} (in solution).[41] On the other hand, acid digestion of $LiMn_2O_4$ or Mn_3O_4 at $25 \le T \le 95$ °C followed by heat treatment at $75 \le T \le 350$ °C gives γ-MnO_2, a mixture of λ- and γ-MnO_2, or β-MnO_2, depending on the reaction conditions.[42] Whereas β-MnO_2 has the rutile structure, γ-MnO_2 has an intergrowth structure consisting of β-MnO_2 domains of relative size (1 × 1) and ramsdellite-MnO_2 domains of size (2 × 1); ramsdellite structure consists of double chains of MnO_6 octahedra with channels of relative dimension (2 × 1).

Similarly, the treatment with acid of Li_2MnO_3 gives $Li_{0.36}Mn_{0.91}O_2$[43] or α-MnO_2[44] stabilized by water molecules. The parent Li_2MnO_3 has a layer structure similar to the $LiCoO_2$ structure in Figure 4, but the Co^{3+} planes are occupied by a combination of 33% Li^+ and 67% Mn^{4+} ions. The removal of lithium oxide in acid from Li_2MnO_3 to give $Li_{0.36}Mn_{0.91}O_2$ involves a shear of the cubic close-packed oxygen planes to create a structure consisting of alternate layers of octahedra and trigonal prisms. However, upon relithiation, a cubic close-packed oxygen array with rock salt structure resembling closely that of layered $LiCoO_2$ is formed for $Li_{1.09}Mn_{0.91}O_2$. The structure of α-MnO_2, on the other hand, consists of interlinking double chains of MnO_6 octahedra with 1-dimensional channels of dimensions (2 × 2) and (1 × 1). α-MnO_2 is known to exist in nature as several minerals, such as cryptomellane (KMn_8O_{16}) and hollandite ($BaMn_8O_{16}$).

The acid treatment procedure, however, results in residual water in all of the aforementioned products. In some cases, such as layered $Li_{0.36}Mn_{0.91}O_2$, heat treatment at moderate temperatures $T \approx 300$ °C to remove water completely causes structural transitions. Both the presence of water and structural instability upon lithium insertion/extraction lead to poor electrochemical properties. Although β-MnO_2, γ-MnO_2, layered $Li_{0.36}Mn_{0.91}O_2$, and α-MnO_2 offer an initial capacity of >200 mA h g^{-1} at 4−2 V, they all tend to lose capacity on electrochemical cycling. Thus, these phases have limitations for use in lithium cells.

Reduction of Permanganate. The ready availability of permanganate and its strong oxidizing nature have prompted the reduction of the permanganate ion with milder reducing agents to obtain new manganese oxides. Accordingly, several groups have focused on the reduction of permanganate with HCl,[45,46] fumaric acid[47,48] sugar,[49] and Mn^{2+} salts[50] in aqueous solutions. These reduction procedures yield hydrated manganese oxides often containing the alkali metal ions. These oxides

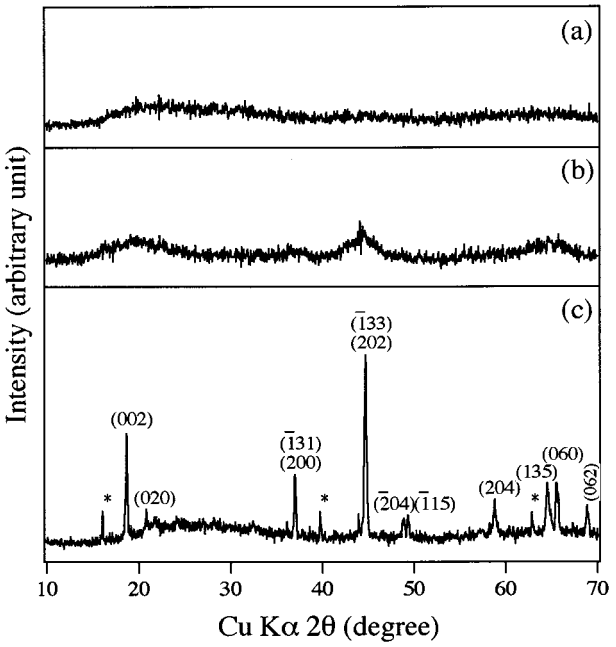

Figure 7. X-ray powder diffraction patterns of the product obtained by reducing sodium permanganate with LiI (1:1.5 ratio) in acetonitrile medium: (a) as prepared sample, (b) after heating under reduced pressure at 250 °C, and (c) after heating in air at 600 °C. The planes marked in (c) refer to Li_2MnO_3 and the * refers to $Na_{0.7}MnO_2$.

have layer structures similar to birnessite,[51] rancieite,[45,46] and $Na_{0.7}MnO_2$,[47] or a hollandite-type α-MnO_2 structure containing Na^+ or K^+ ions in the tunnels.[48,50] Although most of the hydrated oxides show higher capacity (>200 mA h g^{-1} at 4−2 V) at low current densities, they too tend to lose capacity on cycling and, therefore, have limitations. Among these, the hollandite-type α-MnO_2 formed by a reduction of $LiMnO_4$ with $Mn(NO_3)_2$ appears to retain a capacity of ∼150 mA h g^{-1} in the range 4−2 V at moderate current densities after a rapid decline in capacity during the first three cycles.[50]

More recently, the reduction of $AMnO_4$ (A = Li, Na, and K) with water under hydrothermal conditions has been shown to give layered manganese oxides $A_xMnO_2 \cdot nH_2O$ with the TiS_2 structure.[51] Electrochemical studies of these layered oxides after dehydration reveal that the capacity tends to decline upon cycling. The capacity fading is more severe for the lithium compound than for the sodium or potassium compounds. The capacity fading is again due to a transformation of the layered structure to the more stable spinel structure.

Moreover, all the reductions just presented involve aqueous medium, and the products often contain water, which may be undesirable for lithium cells. Accordingly, we recently investigated the reduction of anhydrous $NaMnO_4$ with LiI in acetonitrile medium.[52] The products obtained after heating under reduced pressure at 250 °C were $Li_xNa_yMnO_zI_\eta$ as determined by chemical analysis. The lithium content increases and the sodium and iodine content decrease with increasing LiI in the reaction mixture. The samples heated at 250 °C are amorphous and disproportionate to crystalline Li_2MnO_3 and $Na_{0.7}MnO_2$, with the loss of iodine upon heating at T > 300 °C (Figure 7). The sample fired at 600 °C in Figure 7, for example, does not contain iodine.

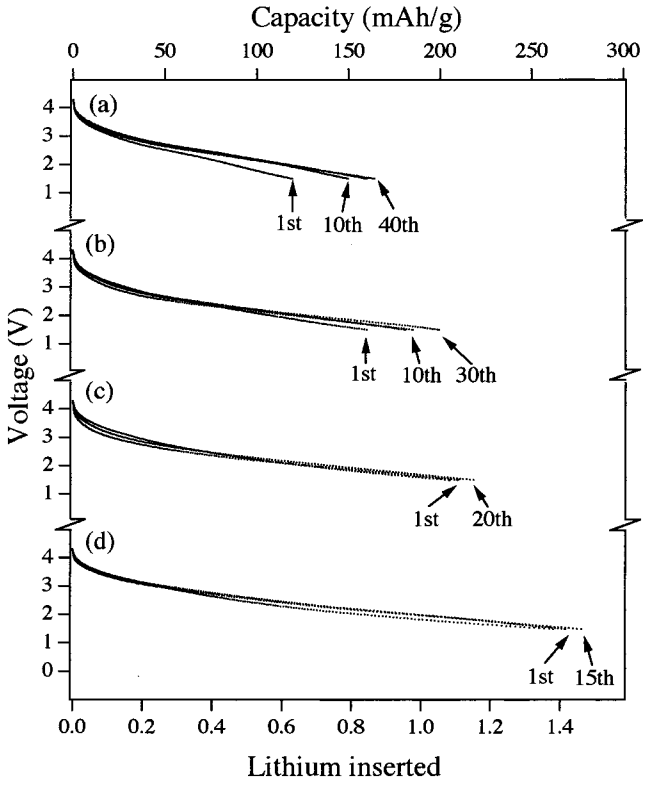

Figure 8. Electrochemical cyclability of amorphous $Li_{1.51}Na_{0.51}MnO_{2.85}I_{0.12}$ that was ball milled with 25 wt % fine carbon for various times: (a) 5 min, (b) 10 min, (c) 20 min, and (d) 40 min. The data were recorded with a current density of 0.5 mA/cm^2 after an initial charge to 4.3 V.

Electrochemical data were collected with the amorphous sample heated under reduced pressure at 250 °C. While the samples prepared with lower amounts of LiI (LiI-to-$NaMnO_4$ ratio of ⩽1.5) show good capacity retention, those prepared with a higher amount of LiI (LiI-to-$NaMnO_4$ ratio of >2) show poor cyclability. Figure 8 shows the cyclability data for the sample $Li_{1.51}Na_{0.51}MnO_{2.85}I_{0.12}$ that was synthesized with a LiI-to-$NaMnO_4$ ratio of ∼1.5. Although our initial published data shows a marked decrease in capacity upon increasing the current density,[52] we have now found that the high capacity of 275 mA h g^{-1} at 4.3−1.5 V can be retained even at higher current densities if the electronic conductivity of these amorphous oxyiodides are enhanced by intimately mixing with carbon. Figure 8 shows the discharge curves recorded after ball milling the oxyiodides with carbon for various periods of time. Higher ball-milling time provides an intimate mixing of carbon and thereby enhances the electrical conductivity in the electrodes and gives higher capacity. The amorphous manganese oxyiodide exhibits the highest capacity involving both the $Mn^{4+/3+}$ and $Mn^{3+/2+}$ couples, with excellent capacity retention among the known manganese oxides. Unlike most of the nonspinel manganese oxides, which have a tendency to transform to the spinel phase upon electrochemical cycling, the amorphous manganese oxyiodide does not transform to the spinel phase. Further spectroscopic work is currently in progress to understand the mechanism of lithium insertion/extraction in these amorphous hosts.

Reduction of permanganate with LiI was also carried out in an aqueous medium.[53] The products obtained after heating in air at T ⩾ 500 °C were $Li_xNa_yMnO_z$ as

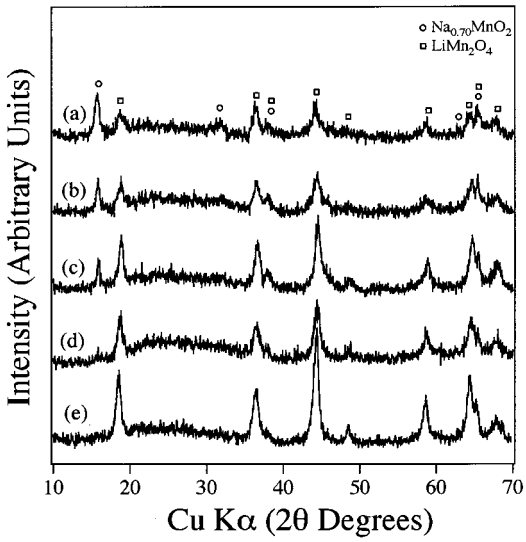

Figure 9. X-ray powder diffraction patterns of the products obtained with various ratios of $NaMnO_4 \cdot H_2O$:$LiI \cdot 3H_2O$ in aqueous medium: (a) 1:0.5 (sample 1), (b) 1:1 (sample 2), (c) 1:2 (sample 3), (d) 1:4 (sample 4), and (e) 1:8 (sample 5). The patterns were recorded after firing the products at 500 °C in air for 3 days.

determined by chemical analysis. Although the as-prepared samples contain some iodine, the samples fired at $T \geq 500$ °C do not contain iodine. The Li/Na ratio in the product increased with increasing amount of lithium iodide in the reaction mixture, as found in the nonaqueous medium. But, the lithium and sodium contents are much lower than that found in the nonaqueous medium for the same conditions. X-ray diffraction data (Figure 9) reveals that the samples, after heating at 500 °C, consist of a mixture of $Li_{1+x}Mn_{2-x}O_{4+\delta}$ spinel and $Na_{0.7}MnO_2$. The lower lithium contents compared with that in the nonaqueous medium leads to the formation of spinel phase rather than Li_2MnO_3. Although the amount of spinel phase increases, that of $Na_{0.7}MnO_2$ decreases with increasing $LiI \cdot 3H_2O$ in the reaction mixture, which is consistent with the increasing Li/Na ratio in the products.

The electrochemical cyclability data of the samples 1−5 (see caption to Figure 9 for details) after firing at 500 °C are shown in Figure 10.[53] Among them, sample 2 provides a capacity of ∼200 mA h g^{-1} at 4.3−2.3 V with excellent cyclability. Although sample 5, with nearly single-phase spinel, exhibits much lower capacity, sample 2, with an optimum amount of the two phases, shows high capacity with excellent cyclability in both the 4 and 3 V regions. The smaller capacity of sample 5 may be due to the differences in microstructure caused by this synthesis procedure. Figure 11 shows the electrochemical performance of sample 2 for various firing temperatures. The sample fired at 500 °C shows the best cyclability. As the firing temperature increases, the cyclability in the 3 V region becomes poor, as found in $LiMn_2O_4$ made by conventional solid-state reaction. Figure 11 also compares the performance of the samples fired at 500 °C in air with that fired at 500 °C first in air and then in N_2. The sample fired in N_2 shows significant capacity in the 4 V region, similar to that of $LiMn_2O_4$ prepared by solid-state reaction at $T > 700$ °C, whereas the sample fired in air shows most of the capacity in the 3 V region, like the cation-deficient spinel

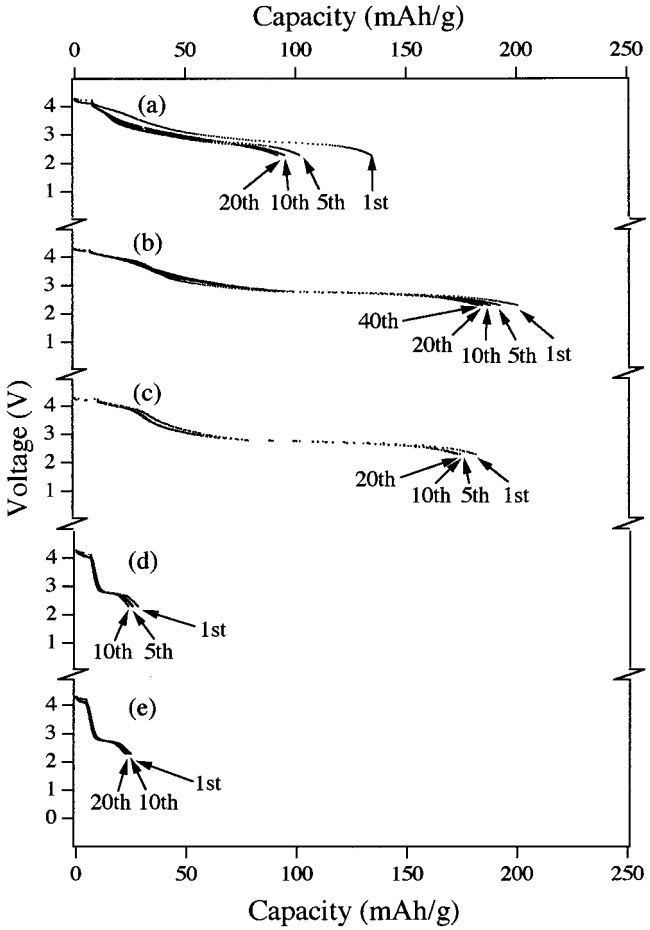

Figure 10. Electrochemical cyclability of the products obtained by the reduction of sodium permanganate with lithium iodide in aqueous medium followed by firing at 500 °C in air for 3 days: (a) sample 1, (b) sample 2, (c) sample 3, (d) sample 4, and (e) sample 5. The data were recorded with a current density of 0.5 mA/cm^2.

$Li_2Mn_4O_9$.[54] This difference is because the spinel phase in the N_2-annealed sample may have an oxygen content close to 4, whereas that in the air-annealed sample may have significant amount of excess oxygen in the spinel $LiMn_2O_{4+\delta}$ (i.e., cation-deficient spinel). The comparison of the air- and N_2-annealed samples proves that the observed capacity retention in the 500 °C samples is not merely due to the higher oxidation state of Mn (i.e., not due to the presence of the spinel phase as, for example, $Li_2Mn_4O_9$ or $Li_4Mn_5O_{12}$) because the N_2-annealed sample that has discharge curves similar to the $LiMn_2O_4$ spinel with plateaus in the 4 and 3 V regions also exhibits excellent capacity retention.

It is clear that the samples with an optimum amount of the two phases with smaller particle size exhibit the best performance. The data demonstrate that the presence of an intimately mixed, second-phase $Na_{0.7}MnO_2$ on a nanometer scale (crystallite size < 10 nm), as revealed by transmission electron micrograph,[53] helps to suppress the problems caused by the lattice distortion and thereby leads to excellent capacity retention in the 3 V region. We believe the strength of the small, adjacent grains of $Na_{0.7}MnO_2$ may introduce local strain fields in such a way that the structural integrity of the electrode is maintained. The situation may be compared with the transformation toughening of zirconia ceramics in which the presence of strong adjacent grains

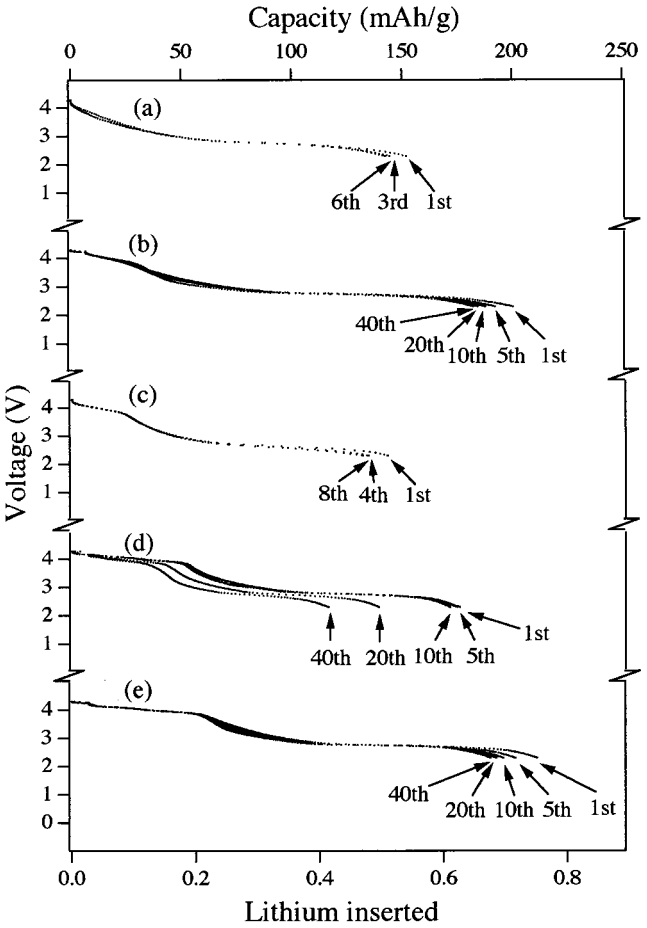

Figure 11. Electrochemical cyclability of sample 2 after firing at various temperatures for 3 days: (a) 400 °C in air, (b) 500 °C in air, (c) 600 °C in air, (d) 700 °C in air, and (e) 500 °C in air followed by in N_2. The data were recorded with a current density of 0.5 mA/cm^2.

of cubic zirconia helps to prevent the volume expansion of small (<0.5 μm) tetragonal zirconia grains.[55]

The data just presented are consistent with several observations[56] that the spinel phase generated during the electrochemical cycling of nonspinel manganese oxides tend to show better cyclability than the conventional single-phase $LiMn_2O_4$; for example, the spinel phase formed during the cycling of orthorhombic $LiMnO_2$ has been found to show better cyclability. Because $Na_{0.7}MnO_2$ is also electrochemically active in our nanocomposite, it helps to maintain a high capacity despite an added weight. This novel nanocomposite strategy thus overcomes the problem associated with the spinel manganese oxides and it may prove useful in utilizing the capacity in the 4 and 3 V regions of the spinel cathodes.

Oxidation of Mn(II). As pointed out earlier, $LiMn_2O_4$ spinel oxides are the most widely investigated manganese oxides. Although the Jahn−Teller distortion associated with Mn^{3+} has plagued $LiMn_2O_4$, this problem can be suppressed by increasing the average oxidation state of manganese through cationic substitutions. Thackeray et al.[9,54] have carried out extensive investigation in this regard; for example, substitution of lithium for manganese in $Li_{1+x}Mn_{2-x}O_4$ increases the average oxidation state of manganese and gives $Li_4Mn_5O_{12}$ as the end member at $x = 0.33$. Although the

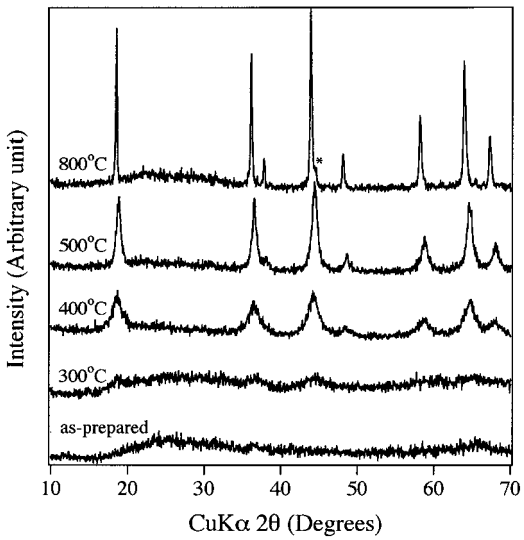

Figure 12. X-ray diffraction patterns of the products obtained by oxidizing Mn^{2+} with lithium peroxide followed by firing at various temperatures. The unmarked reflections refer to $Li_4Mn_5O_{12}$ and * refers to Li_2MnO_3.

increase in the oxidation state of manganese leads to a decrease in capacity in the 4 V region, it leads to a better cyclability in the 3 V region as the Jahn−Teller distortion occurs late in the 3 V region, for example, at $y = 2.5$ in $Li_{4+y}Mn_5O_{12}$. Thus, $Li_4Mn_5O_{12}$ has become an attractive candidate for 3 V batteries. However, $Li_4Mn_5O_{12}$ is unstable to heat treatment and disproportionates to $LiMn_2O_4$ and Li_2MnO_3 at higher temperatures.[54,57] More recently, Thackeray et al.[58] have reported that oxygen begins to be lost above 420 °C, and oxygen is not fully regained on cooling.

$Li_4Mn_5O_{12}$ is generally synthesized by solid-state reaction between manganese oxides or salts and lithium salts at moderate temperatures $T \approx 600$ °C, which leads to oxygen vacancies and/or lower Li content ($x < 0.33$) in $Li_{1+x}Mn_{2-x}O_4$. We have recently developed a low-temperature method involving the oxidation of the aquo ion $[Mn(H_2O)_6]^{2+}$ with lithium peroxide in the presence of excess LiOH at ambient temperature followed by firing the precursor at $T < 500$ °C.[59] Unlike the oxidation of Mn^{2+} with $KMnO_4$ or $K_2S_2O_8$, which leads to the incorporation of alkali metal cations and often to the formation of hollandite-type α-MnO_2 phases,[60] the oxidation with lithium peroxide is cleaner involving only lithium and manganese. The evolution of X-ray diffraction patterns after firing the precursor at various temperatures is shown in Figure 12. The data show that the reflections corresponding to spinel become well defined for $T \geq 400$ °C. More importantly, the progressive movement of reflections to lower angles (Figure 13) with increasing firing temperature, $T > 500$ °C, and the appearance of reflections corresponding to Li_2MnO_3 suggest that $Li_4Mn_5O_{12}$ disproportionates above 500 °C.

Accordingly, electrochemical data (Figure 14) were collected with the samples fired at 400 and 500 °C, which were found to have a manganese oxidation state of, respectively, 3.98+ and 3.97+, with nearly no oxygen vacancies.[59] The sample fired at 400 °C shows an initial capacity of 160 mA h g^{-1} at 3.3−2.3 V, which is close to the theoretical capacity of 163 mA h g^{-1}. Although the 500 °C sample shows a slightly lower initial capacity, it shows better cyclability than the 400 °C sample due

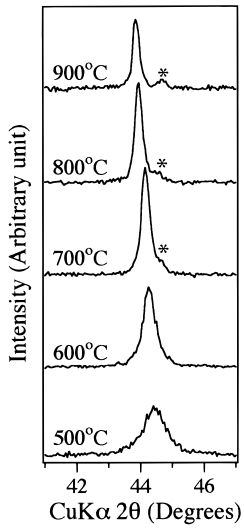

Figure 13. X-ray diffraction patterns of $Li_4Mn_5O_{12}$ over a small two theta range illustrating the movement of diffraction peaks to lower angle with increasing firing temperature.

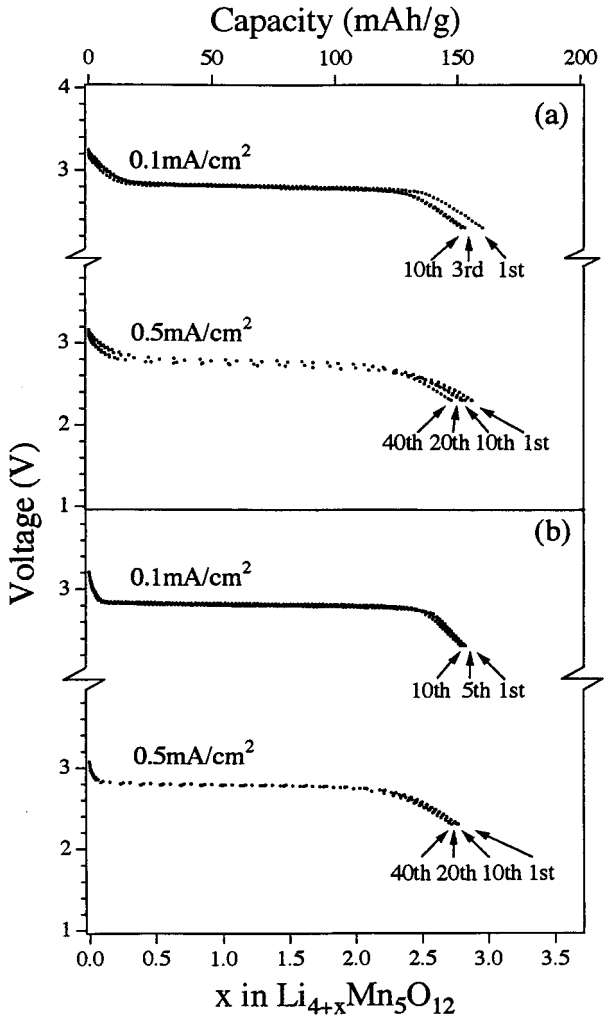

Figure 14. Discharge curves of $Li_4Mn_5O_{12}$ recorded with a current density of 0.1 and 0.5 mA/cm^2: (a) after firing at 400 °C, and (b) after firing at 500 °C.

to better crystallinity. The 500 °C sample shows remarkable capacity retention with < 2% decline over 40 cycles. Both the elimination of oxygen vacancies and a unique microstructure offered by the low-temperature approach lead to the excellent electrochemical properties.

Cobalt and Nickel Oxides

The commercial lithium-ion cells are made with layered $LiCoO_2$ cathodes that are obtained by solid-state reaction at ~850 °C. There has been considerable interest to lower the processing cost by employing low-temperature synthesis procedures. Nickel is less expensive than cobalt, but it tends to form $Li_{1-x}Ni_{1+x}O_2$ with a disordering of Li^+ and $Ni^{3+/2+}$ ions in the Co^{3+} planes of Figure 4 due to the formation of Ni^{2+} at higher temperatures.[23,24] Accordingly, low-temperature procedures have been pursued to synthesize both $LiCoO_2$ and $LiNiO_2$ as well as solid solutions between them.

$LiCoO_2$ has been synthesized by (i) firing a mixture of Li_2CO_3 and $CoCO_3$ at $T = 400$ °C for 1 week,[22] and (ii) a sol−gel process involving cobalt acetate and lithium hydroxide followed by firing at $T \leq 500$ °C.[30,61] However, the low-temperature $LiCoO_2$ formed at $T \leq 500$ °C has a cubic rock salt structure with a disordering of Li^+ and Co^{3+} ions as indicated by solid-state nuclear magnetic resonance (NMR) spectroscopy, X-ray absorption spectroscopy, and high-resolution transmission electron microscopy (TEM).[61] The cation disordering impedes lithium mobility and results in poor electrochemical properties. Similarly, both $Li_{1-x}Ni_{1+x}O_2$ and $Li_{1-x}(Ni_{1-y}Co_y)_{1+x}O_2$ have also been obtained by a sol−gel process involving lithium carbonate and nickel and cobalt nitrates,[62,63] but a higher firing temperature of at least 600 °C is essential to obtain the nickel-containing oxides. The nickel oxides also have cation disordering, which leads to inferior electrochemical properties. However, treatment of $LiMO_2$ (M = Co and Ni) with acid results not only in an extraction of lithium by a disproportionation of M^{3+} to M^{4+} (in solid) and M^{2+} (in solution), but also in a removal of M^{n+} ions from the Li^+ planes, which will improve the cation ordering.[21,64] Although this strategy may appear useful to suppress cation disorder and thereby to achieve smother Li^+ insertion/extraction, the acid treatment involves a partial ion exchange of the Li^+ ions by H^+, which will lead to poor electrochemical behavior.

More recently, ion-exchange reactions of both CoOOH and NiOOH with LiOH under hydrothermal conditions have been shown to give, respectively, $LiCoO_2$ and $LiNiO_2$ at temperatures as low as 100 °C.[65] Unlike the other methods, the hydrothermal method seems to give $LiMO_2$ phases with better crystallinity and cation ordering. However, the use of aqueous medium leads to a contamination of the phases with carbonate and hydroxyl groups as indicated by infrared (IR) spectroscopy. Although the carbonate and hydroxyl groups severely affect the capacity and cyclability, the carbonate and hydroxyl groups could be removed by heating at moderate temperatures $T \approx 250$ °C, at least in the case of $LiCoO_2$. The heat-treated $LiCoO_2$ gives improved electrochemical performance. $LiCoO_2$ has also been produced by firing a freeze-dried hydroxide mixture at temperatures as low as 200 °C.[66] However, the samples fired at lower temperatures show lower capacity and poor cyclability. A firing temperature of 800 °C is necessary to achieve capacity and cyclability comparable to that found with $LiCoO_2$ obtained by the conventional solid-state procedure.

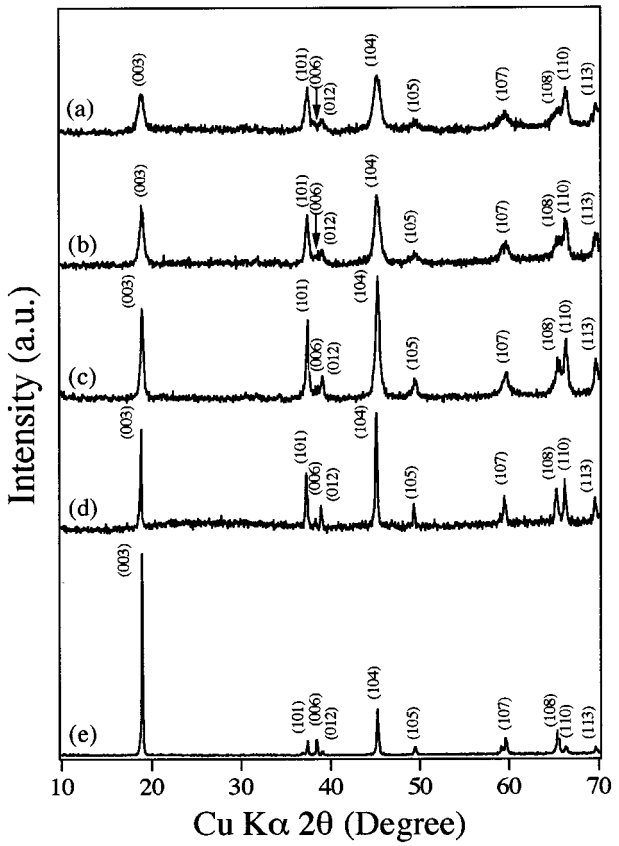

Figure 15. X-ray powder diffraction patterns of the products obtained by oxidizing Co^{2+} with lithium peroxide followed by firing at various temperatures in air and cooling at a rate of 2 °C/min: (a) 400 °C; (b) 500 °C ($Li_{1.1}Co_{0.9}O_{2.04}$); (c) 600 °C; (d) 700 °C ($Li_{1.09}Co_{0.91}O_{2.03}$); and (e) 900 °C ($Li_{0.99}CoO_2$).

We have extended the peroxide oxidation reactions adopted for manganese spinels to $LiCoO_2$ as well. The oxidation of the aquo ion $[Co(H_2O)_6]^{2+}$ with lithium peroxide in the presence of excess LiOH followed by firing the precursor at $T \geq 400$ °C yields lithium cobalt oxides.[67] Figure 15 shows the X-ray diffraction patterns along with chemical compositions for various firing temperatures. Although samples with a Li/Co ratio of >1.0 could be obtained at lower firing temperatures, only stoichiometric $LiCoO_2$ with a Li/Co ratio of 1.0 is obtained at firing temperatures of $T \approx 900$ °C. As discussed earlier, stoichiometric $LiCoO_2$ is known to be formed as a disordered material when synthesized at lower temperatures $T \leq 500$ °C.[22,30,61] The compositions given in Figure 15 reveal that although the disordered or less crystalline samples can accommodate a Li/Co ratio of >1, the ordered material formed at 900 °C tends to have a Li/Co ratio of 1.0. It was found that the *a* parameter does not vary significantly, but the *c* parameter decreases with increasing firing temperature. Although the *c* parameter of the 900 °C sample (14.047 Å) agrees well with the literature value (14.059 Å), that of the 400 °C sample (14.098 Å) differs markedly from that reported (13.87 Å) for a $LiCoO_2$ sample synthesized by firing a mixture of Li_2CO_3 and $CoCO_3$ at $T = 400$ °C for 1 week.[22] The difference is because of the substitution of a larger Li^+ ions for the smaller Co^{3+} ions because the 400 °C sample in our investigation has a Li/Co ratio of >1.

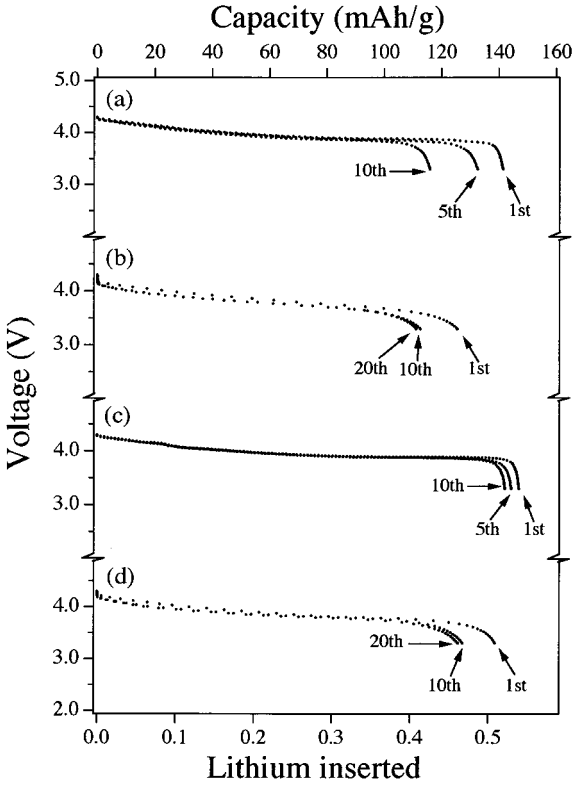

Figure 16. Electrochemical cyclability of $LiCoO_2$ after firing at various temperatures: (a) 700 °C, 0.1 mA/cm^2; (b) 700 °C, 0.5 mA/cm^2; (c) 900 °C, 0.1 mA/cm^2; and (d) 900 °C, 0.5 mA/cm^2.

The samples synthesized at $T < 600$ °C showed poor electrochemical properties due to the disordering of the Li^+ and Co^{3+} ions in the layer structure of $LiCoO_2$ (Figure 4). Figure 16 shows the cyclability of the samples fired at 700 and 900 °C with different current densities. The 900 °C sample shows better performance than the 700 °C sample because of better crystallinity and crystallographic ordering, which is consistent with other studies.[22,61] It is clear from the results of various studies that a firing temperature of $T \geq 800$ °C is essential to obtain good electrochemical properties, and thus the low-temperature approach may not provide any significant advantage in the case of $LiCoO_2$.

Iron Oxides

From both cost and toxicity points of view, iron oxides are preferred over other transition metal oxide hosts. Unfortunately, $LiFeO_2$ obtained by convention solid-state procedures does not adopt the layer structure of $LiCoO_2$. However, layered $LiFeO_2$ has been produced by (i) an ion exchange of layered $NaFeO_2$ with molten lithium salts such LiCl, LiBr, LiI and $LiNO_3$,[35] and (ii) hydrothermal reaction between α-FeOOH or $FeCl_3 \cdot 6H_2O$ and mixed alkaline solutions consisting of LiOH−NaOH or LiOH−KOH.[68] But, the layered $LiFeO_2$ exhibits poor electrochemical properties, possibly due to the migration of iron to lithium planes. Attempts to substitute iron for nickel in $LiNi_{1-y}Fe_yO_2$ reveal that only a small amount ($y < 0.23$) of iron could be substituted while maintaining the $LiNiO_2$ structure and the cell capacity decreases with increasing y.[69]

On the other hand, an ion exchange reaction of γ-FeOOH with LiOH under hydrothermal conditions at

100−250 °C has been shown[70] to give new form of $LiFeO_2$ that is isostructural with the orthorhombic $LiMnO_2$. This new form consists of corrugated layers of the FeO_6 and LiO_6 octahedra that are not parallel to the close-packed oxygen layers. Electrochemical studies reveal that the orthorhombic $LiFeO_2$ is, however, unstable to lithium extraction and it transforms to an amorphous phase. Although the subsequent cycling shows moderate capacity retention, the overall cell capacity is <100 mA h g^{-1} in the range 1.5−3.5 V and thus it may not compete with $LiCoO_2$ cathodes.

Vanadium Oxides

Although $LiVO_2$, with the layer structure shown in Figure 4, can be readily made, the vanadium atoms migrate into the lithium planes upon extracting >0.33 Li.[71] Therefore, the layered $LiVO_2$ is not a promising cathode. Vanadium forms a number of binary oxides with general formula VO_{2+x} in addition to the well-known V_2O_5 and V_2O_3. The oxides VO_2, V_6O_{13}, V_4O_9, and V_3O_7, with x values of, respectively, 0, 0.17, 0.25, and 0.33, are members of the VO_{2+x} ($0 \le x \le 0.33$) family. The VO_{2+x} phases have shear structures derived from a hypothetical VO_3 with the ReO_3 structure. The structure consists of distorted VO_6 octahedra sharing both corners and edges.[72] The VO_2 with this shear structure with a 1-dimensional tunnel is metastable and has been designated as VO_2(B). Among the VO_{2+x} phases, only V_6O_{13} and VO_2(B) were initially found to show promising electrochemical properties.[73] Subsequently, V_6O_{13} has been investigated extensively, particularly for lithium polymer batteries, but VO_2(B) remains relatively less studied because it could insert only ~0.5 Li per V.

We identified recently that the hard to reduce oxo ions $(MO_4)^{n-}$, such as $(VO_4)^{3-}$, $(CrO_4)^{2-}$, and $(MoO_4)^{2-}$, can be reduced in aqueous solution with a stronger reducing agent like the alkali metal borohydrides ABH_4 (A = Na or K).[74] The borohydride ion hydrolyzes in aqueous solutions to give hydrogen as

$$BH_4^- + 2H_2O \rightarrow BO_2^- + 4H_2 \qquad (3)$$

and the hydrolysis reaction is facilitated by acidic conditions.[75] A more systematic investigation of the reduction of vanadates,[76] chromates,[77] permanganates,[78] molybdates,[79] and tungstates[80] reveals that both the binary oxides MO_z and the ternary oxides $A_xM_yO_z$ could be obtained depending on the reaction conditions, such as the reaction pH and concentration and amount of the reactants. Although the reducing power of borohydride increases with decreasing pH,[75] the increasing degree of condensation of the oxo ions with decreasing pH to give poly anions[81] leads to a complex dependence of the reduction products on pH because the condensed poly anions are more difficult to reduce than the monomeric $(MO_4)^{n-}$ ions.

The chemical reaction for the formation of the binary oxide VO_2 can be given as

$$2K_3VO_4 + 2KBH_4 + 6H_2O \rightarrow 2KBO_2 + 2VO_2 + 6KOH + 7H_2 \qquad (4)$$

The VO_2 obtained was the metastable VO_2(B) and it transforms irreversibly to the thermodynamically more stable rutile structure at T > 300 °C, as revealed by the X-ray diffraction.[82] This transformation was accompanied by an exothermic peak in differential scanning calorimetry (DSC) plot. The as-prepared sample contained some water, and the water is lost below ~250 °C, as revealed by thermogravimetric analysis (TGA) data.[82] The electrochemical data were, therefore, collected with the sample that was heated under reduced pressure at 240 °C for 2 h to remove the water. The vacuum-annealed sample was nanocrystalline as indicated by TEM.

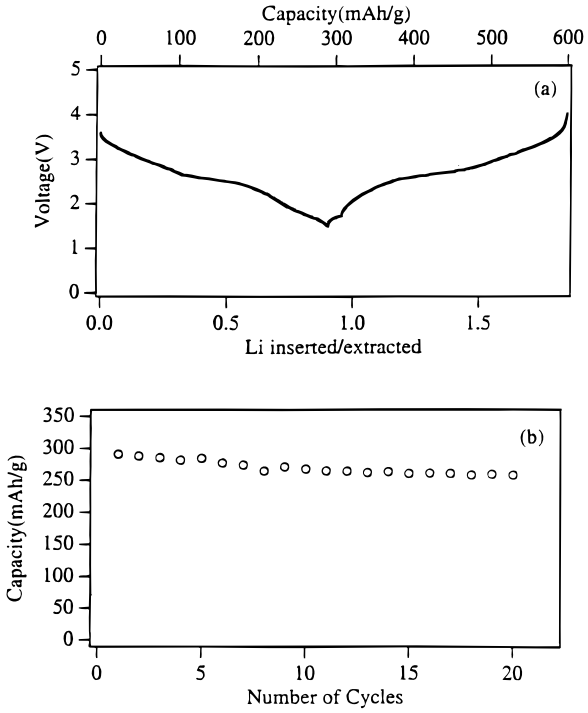

Figure 17. (a) Discharge−charge curve and (b) cyclability of nanocrystalline VO_2(B), recorded with a current density of 0.5 mA/cm^2.

The discharge−charge curves and cyclability of nanocrystalline VO_2(B) are shown in Figure 17. The data show a capacity of ~290 mA h g^{-1} at 4−1.5 V, corresponding to a lithium insertion/extraction of 0.9 Li per V, with excellent cyclability. The observed capacity is much higher than that reported in the literature (~0.5 Li per V) from both electrochemical (above a cutoff voltage of 1.5 V) and chemical lithium insertion experiments.[73] The literature method involves a controlled and careful reduction of NH_4VO_3 or V_2O_5 with gases such as H_2, NH_3, or SO_2 at 200 < T < 537 °C.[72,73,83] We believe the smaller particle size (<100 nm) achieved by the solution-based approach and the accompanying microstructure play a critical role in giving higher capacity and better electrode properties. In addition, VO_2(B) is tedious to synthesize as a single-phase material by the literature procedures. The borohydride reduction method is simple and readily gives single-phase material. Moreover, VO_2(B) has been suggested to be an anode for lithium cells employing aqueous electrolytes.[84]

A VO_2 with the composition $Li_{0.6}V_{2-\delta}O_{4-\delta}\cdot H_2O$ has been synthesized by hydrothermal reaction of V_2O_5 and LiOH in the presence of $[N(CH_3)_4]^+$ as a templating

cation.[85] It has a layer structure with square pyramidal coordination for vanadium. After removing the water by heat treatment at 150 °C and extracting the lithium electrochemically, a new form of VO_2 could be obtained. The VO_2 thus obtained reversibly inserts 0.7 Li per V at 4−2 V at low current densities.

Recently, phase-pure V_6O_{13} has been synthesized by a thermal decomposition of NH_4VO_3 in a specially designed reaction chamber that allows a maximum overpressure of 1.5 MPa at a heating rate of 0.5 °C/min between 25 and 500 °C.[86] Electrochemical data and in situ X-ray diffraction analysis of thin-film polymer electrolyte cells reveal the formation during discharge of four $Li_xV_6O_{13}$ phases, with $x = 0.5$, 1.5, 3, and 6, that are similar to that found from chemical lithiation. Whereas phase-pure V_6O_{13} exhibits excellent cyclability, the presence of a V_2O_5 impurity degrades the electrochemical performance.

In addition to the VO_{2+x} phases, both V_2O_5 and LiV_3O_8 containing V^{5+} ions show interesting electrochemical properties. Recently, xeogel and aerogel forms of V_2O_5 that are dominantly amorphous have been investigated.[87,88] Although thin-film xerogel electrodes show high capacity with an insertion of 4 Li per V_2O_5,[87] thick composite pellet electrodes fabricated with xerogels show much lower capacity, with <2 Li per V_2O_5;[88] these xerogels were synthesized, for example, by a sol−gel processing of H^+-exchanged sodium metavanadate. On the other hand, a V_2O_5 sample synthesized by oxidizing metallic vanadium with hydrogen peroxide has a structure intermediate between well crystalline and amorphous V_2O_5 and shows a slightly higher capacity with 2.1 Li per V_2O_5.[89] Layered LiV_3O_8 obtained by sol−gel reactions between V_2O_5 and LiOH show a reversible insertion of 4 Li per formula unit with good cyclability.[90] It has been shown that the capacity of LiV_3O_8 can be increased by ∼60% by ultrasonically treating the samples.[91] The increase in capacity has been attributed to decrease in crystallinity and an increase in surface area and interlayer spacing. Recently, amorphous hydrated RVO_4 oxides, with R = Fe and In, that are synthesized by a precipitation reaction between ammonium vanadate and iron or indium nitrates have been shown to exhibit reversible capacities of as large as 900 mA h g^{-1} at 3−0.2 V, with about 15 Li per formula unit.[92] These oxides have been suggested to be of potential interest as anodes. Clearly, crystallinity, particle size, and microstructure that are strongly controlled by synthesis and processing procedures play a critical role in the electrochemical properties of vanadium oxides.

Chromium Oxides

A number of chromium oxides such as Cr_2O_3, CrO_2, Cr_5O_{12}, Cr_2O_5, Cr_6O_{15}, and Cr_3O_8 have been investigated as electrode materials.[93−95] Among them, both Cr_2O_3 and CrO_2, with Cr valences of ≤4+, showed poor capacity and lower energy densities. In contrast, Cr_2O_5, Cr_6O_{15}, and Cr_3O_8, with Cr valences of ≥5+, showed larger capacities and energy densities as high as 1200 W h/kg above a cutoff voltage of 2 V.[94] In addition, amorphous Cr_3O_8 showed a maximum theoretical energy density of 1800 W h/kg, with good rechargeability.[95] These chromium oxides, excepting Cr_2O_3, are generally synthesized by decomposition of CrO_3 in an autoclave or under high oxygen pressure,[96] and the products are often contaminated with undecomposed CrO_3.

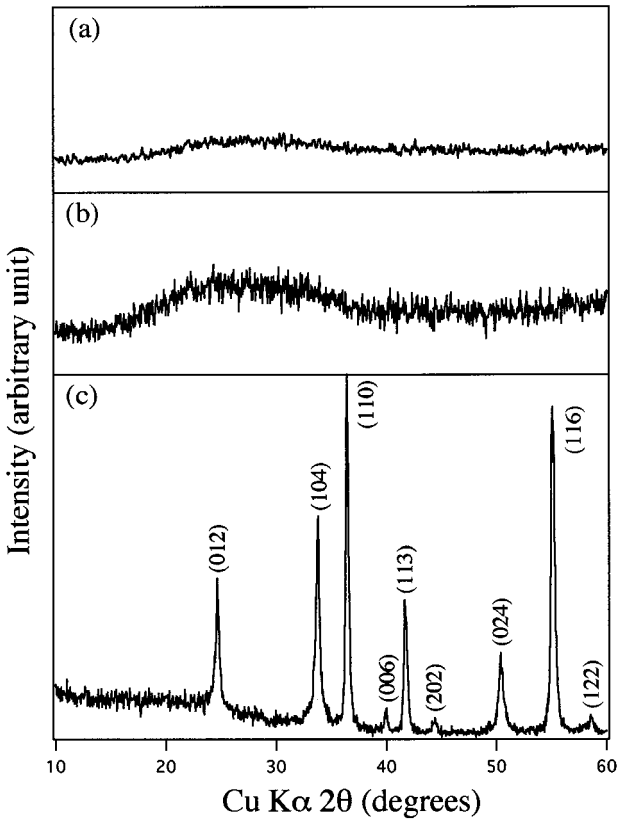

Figure 18. X-ray diffraction patterns of CrO_2: (a) after drying in air-oven at 110 °C (amorphous $CrO_2 \cdot xH_2O$); (b) after heating in TGA in N_2 atm to 350 °C (amorphous CrO_2); and (c) after heating in TGA in N_2 atm to 450 °C (crystalline Cr_2O_3).

We have utilized the borohydride reduction method described earlier to obtain chromium oxides.[77] Reduction of K_2CrO_4 with KBH_4 gives the binary oxides $CrO_{2-\delta}$, with $0 \le \delta \le 0.5$. The oxygen content $(2 - \delta)$ and the oxidation state of chromium decrease with increasing volume of KBH_4 at a given pH or with increasing pH at a given amount of KBH_4. The as-prepared, amorphous $CrO_{2-\delta}$ for $\delta < 0.5$ first lose oxygen sharply at $370 < T < 600$ °C and then crystallize immediately to give Cr_2O_3 as indicated by X-ray diffraction (Figure 18) and thermal analysis data (Figure 19). The gradual weight loss below 350 °C in the thermogravimetric analysis (TGA) plot in Figure 19 corresponds to the loss of water, whereas the sharp weight loss around 430 °C corresponds to the loss of oxygen, which is accompanied by an exotherm in differential scanning calorimetry (DSC). The oxygen loss temperature was found to increase monotonically from 370 °C for $\delta = 0$ to 600 °C for δ close to 0.5.

The electrochemical behavior of amorphous $CrO_{2-\delta}$ samples obtained after heating under reduced pressure at 250−300 °C to remove water was investigated.[77] The capacity of amorphous $CrO_{2-\delta}$ decreases with increasing δ due to a decreasing oxidation state of chromium. The discharge−charge curves of the $\delta = 0$ sample, CrO_2, are given in Figure 20 for two current densities. With a current density of 0.1 mA/cm^2, an initial capacity of 180 mA h g^{-1} in the range 3.3−2.3 V is shown, which corresponds to an insertion of about 0.6 Li per Cr. Upon

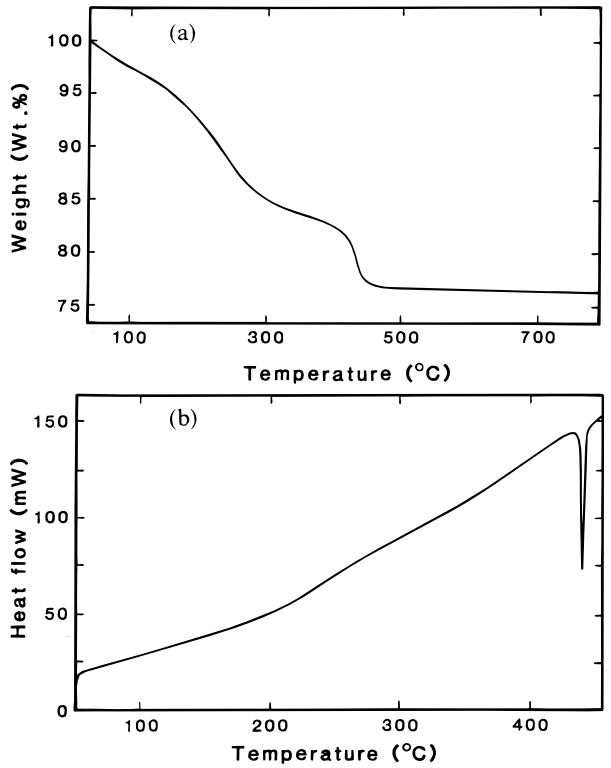

Figure 19. (a) TGA, and (b) DSC plots of CrO_2 recorded in N_2 atmosphere.

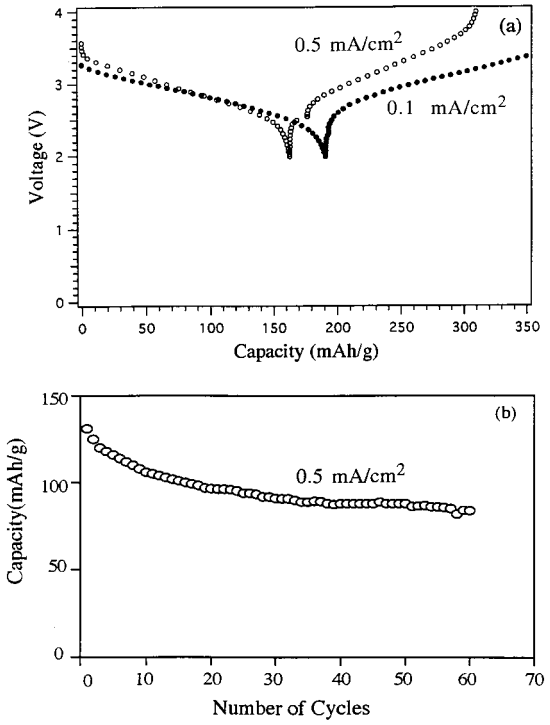

Figure 20. (a) Discharge−charge curves and (b) cyclability of amorphous CrO_2.

increasing the current density to 0.5 mA/cm^2, the initial capacity decreases to ~150 mA h g^{-1}. The cyclability of CrO_2 collected with a current density of 0.5 mA/cm^2 reveals that the capacity tends to stabilize around 90 mAh/g after an initial decline during the first 20 cycles. Further optimization of synthesis procedure may improve the electrochemical properties. The electrochemical behavior of amorphous CrO_2 differs distinctly from

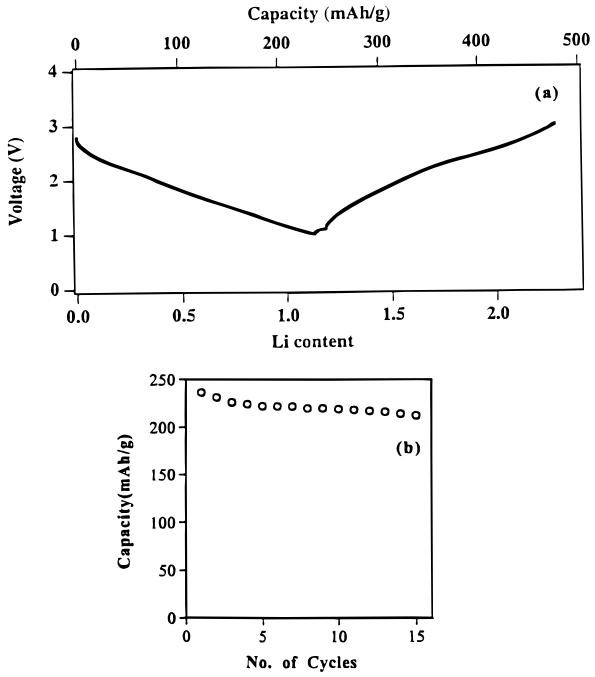

Figure 21. (a) Discharge−charge curves and (b) cyclability of amorphous $MoO_{2.3}$, recorded with a current density of 0.5 mA/cm^2.

that of crystalline CrO_2. The former shows a capacity of 150 mA h g^{-1} in the range 3.3−2.3 V, whereas the latter shows a capacity of 50 mA h g^{-1} in the range 3−1 V for the same current density.[94]

Other Oxides

Titanium Oxides. Whereas layered $LiTiO_2$ is difficult to synthesize, spinel $LiTi_2O_4$ has much lower voltage (1.4 V) and smaller capacity.[97] Recently, anatase TiO_2 synthesized by (i) hydrolysis of titanium alkoxides followed by autoclaving at ~200 °C,[98] and (ii) oxidation of metallic Ti or TiC with hydrogen peroxide followed by firing at 400 °C[99] have been investigated. The anatase exhibits discharge curves around 1.5 V. The presence of carbon in the samples obtained by the oxidation of TiC with hydrogen peroxide leads to much higher capacity than that obtained for the sample synthesized from titanium.

Molybdenum Oxides. We have utilized the borohydride reduction to obtain amorphous molybdenum oxides as well. The $MoO_{2.3}$ obtained after heating the as-prepared sample under reduced pressure at 300 °C to remove water was amorphous as revealed by X-ray diffraction and TEM.[100] This oxide loses oxygen and transforms irreversibly to the rutile MoO_2 upon heating to 370 °C, as revealed by an exotherm in the DSC plot and weight loss determined by TGA. The discharge−charge curves and cyclability of amorphous $MoO_{2.3}$ are shown in Figure 21: a reversible capacity of ~220 mA h g^{-1}, corresponding to an insertion of 1.1 Li per Mo, with good cyclability in the range 3−1 V is shown.

Tin Oxides. The consideration of tin oxides as anodes for lithium-ion batteries by Fuji Photo Film Company has drawn interest in the solution-based synthesis of tin oxides. A sol−gel process involving the reaction between stannic chloride and lithium hydroxide has been utilized to obtain nanometer size SnO_2 with homogeneous particle size distribution.[101,102]

A reversible capacity of as high as 600 mA h g^{-1} at 2−0 V has been found with samples fired at 800 °C,[102] which is much higher than that achieved with graphite (372 mA h g^{-1}). However, the SnO_2 electrodes exhibits very high capacity loss during the first discharge. Several groups have investigated the mechanism of lithium insertion to account for the high capacity.[102,103] The following two-step reaction process has been proposed: first an irreversible reaction of Li^+ with SnO_2 to give Sn and Li_2O, which corresponds to an irreversible capacity of 700 mA h g^{-1}, and then a reversible reaction of Sn with Li^+ to give Li_ySn alloys, which corresponds to a reversible capacity of 600 mA h g^{-1} for $y = 3.4$. The Li_2O formed during the first irreversible process has been suggested to play an important role in the subsequent reversibility of the electrodes.

Conclusions

The use of "rocking chair" concept with insertion compounds as both cathode and anode hosts has made rechargeable lithium batteries a commercial reality. But the cost and environmental concerns of the cobalt oxide has created concerted efforts both to improve the performance of manganese oxides and to develop new insertion oxides. Several low-temperature synthesis procedures such as sol−gel processing, ion-exchange reactions, hydrothermal reactions, and oxidation−reduction reactions in solutions have been pursued. These soft chemistry approaches have accessed several metastable phases with interesting electrochemical properties. However, the incorporation of water in products obtained by aqueous methods and the structural and chemical stability of metastable phases on prolonged electrochemical cycling pose difficulties in some cases.

The cost and environmental benefits have directed a vast portion of the research efforts toward manganese oxides. Although several metastable phases, such as the layered $LiMnO_2$, have been accessed by low-temperature procedures, the transformation of Li−Mn−O oxides under electrochemical cycling to spinel-like phases and the anisotropic lattice (Jahn−Teller) distortion in the spinel oxide have plagued manganese oxides. This difficulty remains to be a challenge to solid-state chemists, and intuitive design and accessibility of structures, compositions, or microstructures that can suppress such problems may prove useful. Synthesis of amorphous compositions in nonaqueous media seems to be promising in this regard.[52] Alternatively, oxides with nonclose-packed structures, which can avoid the transformation to spinel-like phase, could prove to overcome this difficulty.

Iron oxides will also be preferred from cost and environmental points of view, but the layered iron oxides do not exhibit promising electrochemical properties. Although layered $LiNiO_2$ is difficult to achieve as a perfect ordered material, partial substitution of cobalt for nickel in $LiNi_{0.85}Co_{0.15}O_2$ by solid-state reactions seems to give good cyclability with capacity as high as 180 mA h g^{-1}.[104] A few vanadium oxides show high capacity, but from an environmental point of view, they may not be able to compete. Titanium oxides, on the other hand, exhibit lower voltages and are not attractive for cathodes. The recent results with tin oxides appear to be promising and tin oxides can compete with carbon anodes in lithium-ion cells.

In conclusion, innovative synthesis and processing procedures remain the key in developing successful electrode hosts. Synthetic solid-state chemistry has a profound role to play in this strategy. Development of high-energy-density batteries with low-cost, environmentally benign electrode hosts will have a significant impact in consumer electronics and perhaps in zero-emission cars.

Acknowledgment. Financial support by the Welch Foundation Grant F-1254 and National Science Foundation Grant DMR-9401999 is gratefully acknowledged.

References

(1) Scrosati, B. *Nature* **1995**, *373*, 557.
(2) Lave, L. B.; Henrickson, C. T.; McMichael, F. C. *Science* **1995**, *268*, 993.
(3) Goodenough, J. B. *Solid State Ionics* **1994**, *69*, 184.
(4) Aydinol, M. K.; Ceder, G. *J. Electrochem. Soc.* **1997**, *144*, 3832.
(5) *Lithium Battery Energy Storage (LIBES) Publication*, Technological Research Association: Tokyo, 1994.
(6) Whittingham, M. S.; Jacobson, A. J. *Intercalation Chemistry*, Academic: New York, 1982; Gabano, J. P. *Lithium Batteries*, Academic: London, 1993; Venkatasetty, H. V. *Lithium Battery Technology*, John Wiley & Sons: New York, 1984.
(7) Hewston, T. A.; Chamberland, B. L. *J. Phys. Chem.* **1987**, *48*, 97; Murphy, D. W. *Advances in the Synthesis and Reactivity of Solids*; Mallouk, T. E., Ed.; Jai: Greenwich, CT, 1991; Vol. 1, p 237; *Lithium Batteries: New Materials, Developments and Perspectives*, Pistoia, G., Ed.; Elsevier: Amsterdam, 1994; Vol. 5.
(8) Linden, D. *Handbook of Batteries*, 2nd ed.; Linden, D., Ed.; McGraw-Hill: New York, 1995; p 14.1.
(9) Thackeray, M. M. *Prog. Solid State Chem.* **1997**, *25*, 1.
(10) Goodenough, J. B.; Manthiram, A.; James, A. C. W. P.; Strobel. P. *Mater. Res. Soc. Symp. Proc.* **1989**, *135*, 391.
(11) Mizushima, K.; Jones, P. C.; Wiseman, P. J.; Goodenough, J. B. *Mater. Res. Bull.* **1980**, *15*, 783; Goodenough, J. B.; Mizushima, K.; Takeda, T. *Jpn. J. Appl. Phys.* **1980**, *19*, 305.
(12) Thackeray, M. M.; David, W. I. F.; Bruce, P. G.; Goodenough, J. B. *Mater. Res. Bull.* **1983**, *18*, 461.
(13) Dyer, L. D.; Borie, B. S., Jr.; Smith, G. P. *J. Am. Chem. Soc.* **1954**, *76*, 1499.
(14) Scrosati, B.; Megahed, S. Electrochemical Society Short Course, New Orleans, October 10, 1993. Hossain, S. *Handbook of Batteries*, 2nd ed.; Linden, D., Ed.; McGraw-Hill: New York, 1995; p 36.1.
(15) Manthiram, A.; Goodenough, J. B. *J. Power Sources* **1989**, *26*, 403; Okada, S.; Nanjundaswamy, K. S.; Manthiram, A.; Goodenough, J. B.; Ohtsuka, H.; Arai, H.; Yamaki, J. *Proceedings of the 36th Power Sources Conference*; Nedell, R., Ed.; U. S. Army Research Laboratory: Cherry Hill, NJ, 1994; p 110.
(16) Nagaura, T. *JEC Battery Newsletter* **1991**, *2*, 2-1.
(17) Aurbach, D.; Ein-Eli, Y.; Chusid, O.; Carmeli, Y.; Babai, M.; Yamin, H. *J. Electrochem. Soc.* **1994**, *141*, 603; Kanamura, K.; Shirashi, S.; Takehara, Z. *J. Electrochem. Soc.* **1994**, *141*, L108.
(18) Mohri, M.; Yanagisawa, N.; Tajima, Y.; Tanaka, H.; Miyake, T.; Nakajima, S.; Yoshida, M.; Yoshimoto, Y.; Suzuki, T.; Wada, H. *J. Power Sources* **1989**, *26*, 545; Nishi, Y.; Azuma, H.; Omaru, A. U.S. Patent 4959281, 1990; Tarascon, J. M.; Guyomard, D. *J. Electrochem. Soc.* **1991**, *138*, 2864.
(19) Dahn, J. R.; Fong, R.; Spoon, M. J. *Phys. Rev.* **1990**, *B42*, 6424; Ozawa, K. *Solid State Ionics* **1994**, *69*, 212.
(20) Reimers, J. N.; Dahn, J. R. *J. Electrochem. Soc.* **1992**, *139*, 2091; Ohzuku, T.; Ueda, A.; Nagayama, M.; Iwakashi, Y.; Komori, H. *Electrochim. Acta* **1993**, *38*, 1159; Amatucci, G. G.; Tarascon, J. M.; Klein, L. C. *J. Electrochem. Soc.* **1996**, *143*, 1114.
(21) Gupta, R.; Manthiram, A. *J. Solid State Chem.* **1996**, *121*, 483.
(22) Gummow, R. J.; Thackeray, M. M.; David, W. I. F.; Hull, S. *Mater. Res. Bull.* **1992**, *27*, 327.
(23) Dutta, G.; Manthiram, A.; Goodenough, J. B. *J. Solid State Chem.* **1992**, *96*, 123.
(24) Hirano, A.; Kanno, R.; Kawamoto, Y.; Takeda, Y.; Yamamura, K.; Takano, M.; Ohyama, K.; Ohashi, M.; Yamaguchi, Y. *Solid State Ionics* **1995**, *78*, 123.
(25) Megahed, S.; Scrosati, B. *J. Power Sources* **1994**, *51*, 79; Thackeray, M. M. *J. Electrochem. Soc.* **1995**, *142*, 2558; Koksbang, R.; Barker, J.; Shi, H.; Saidi, M. Y. *Solid State Ionics* **1996**, *84*, 1.
(26) Stein, A.; Keller, S. W.; Mallouk, T. E. *Science* **1993**, *259*, 1558.

(27) Livage, J.; Henry, M.; Sanchez, C. *Prog. Solid State Chem.* **1988**, *18*, 259.
(28) Manthiram, A.; Goodenough, J. B. *Nature* **1987**, *329*, 701.
(29) Shen, Y. F.; Zerger, R. P.; DeGuzman, R. N., Suib, S. L.; Mccurdy, L.; Potter, D. I.; O'Young, C. L. *Science* **1993**, *260*, 511.
(30) Barboux, P.; Tarascon, J. M.; Shokoohi, F. K. *J. Solid State Chem.* **1991**, *94*, 185.
(31) Chen, L.; Huang, X.; Kelder, E.; Schoonman, J. *Solid State Ionics* **1995**, *76*, 91.
(32) Huang, H.; Bruce, P. G. *J. Electrochem. Soc.* **1994**, *141*, L106.
(33) Hernan, L.; Morales, J.; Sanchez, L.; Sanyos, J. *Solid State Ionics* **1997**, *104*, 205.
(34) Liu, W.; Farrington, G. C.; Chaput, F.; Dunn, B. *J. Electrochem. Soc.* **1996**, *143*, 879.
(35) Fuchs, B.; Kemmler-Sack, S. *Solid State Ionics* **1994**, *68*, 279.
(36) Armstrong, A. R.; Bruce, P. G. *Nature* **1996**, *381*, 499; Vitins, G.; West, K. *J. Electrochem. Soc.* **1997**, *144*, 2587.
(37) Capitaine, F.; Gravereau, P.; Delmas, C. *Solid State Ionics* **1996**, *89*, 197.
(38) Delmas, C.; Capitaine, F. *Abstract of the 8th International Meeting on Lithium Batteries* **1996**, *8*, 470.
(39) Ohzuku, T.; Ueda, A.; Hirai, T. *Chem. Express* **1992**, *7*, 193; Reimers, J. N.; Fuller, E. W.; Rossen, E.; Dahn, J. R. *J. Electrochem. Soc.* **1993**, *140*, 3396; Pistoia, G.; Antonini, A.; Zane, D. *Solid State Ionics* **1995**, *78*, 115.
(40) Doeff, M. M.; Richardson, T. J.; Kepley, L. *J. Electrochem. Soc.* **1996**, *143*, 2507.
(41) Hunter, J. C. *J. Solid State Chem.* **1981**, *39*, 142.
(42) Thackeray, M. M.; De Kock, A. *J. Solid State Chem.* **1988**, *74*, 414; Thackeray, M. M.; De Kock, A.; De Picciotto, L. A. *J. Power Sources* **1989**, *26*, 355.
(43) Rossouw, M. H.; Thackeray, M. M. *Mater. Res. Bull.* **1991**, *26*, 463.
(44) Rossouw, M. H.; Liles, D. C.; Thackeray, M. M.; David, W. I. F.; Hull, S. *Mater. Res. Bull.* **1992**, *27*, 221.
(45) Tsuji, M.; Komarneni, S.; Tamaura, Y.; Abe, M. *Mater. Res. Bull.* **1992**, *27*, 741.
(46) Leroux, F.; Guyomard, D.; Piffard, Y. *Solid State Ionics* **1995**, *80*, 299; **1995**, *80*, 307.
(47) Bach, S.; Pereira-Romos, J. P.; Baffier, N. *Solid State Ionics* **1995**, *80*, 151.
(48) Le Goff, P.; Baffier, N.; Bach, S.; Pereira-Romos, J. P.; Messina, R. *Solid State Ionics* **1993**, *61*, 309.
(49) Ching, S.; Landrigan, J.; Jorgensen, M.; Duan, D.; Suib, S. L.; O'Young, C. *Chem. Mater.* **1995**, *7*, 1604.
(50) Feng, Q.; Kanoh, H.; Ooi, K.; Tani, M.; Nakacho, Y. *J. Electrochem. Soc.* **1994**, *141*, L135.
(51) Chen, R.; Zavalij, P. Y.; Whittingham, M. S. *Chem. Mater.* **1996**, *8*, 1275; Chen, R.; Whittingham, M. S. *J. Electrochem. Soc.* **1997**, *144*, L64.
(52) Kim, J.; Manthiram, A. *Nature* **1997**, *390*, 265.
(53) Kim, J.; Manthiram, A. *Electrochem. Solid State Lett.* In press.
(54) Thackeray, M. M.; De Kock, A.; Rossouw, M. H.; Liles, D. C.; Hoge, D.; Bittihn, R. *J. Electrochem. Soc.* **1992**, *139*, 363; Gummow, R. J.; De Kock, A.; Thackeray, M. M. *Solid State Ionics* **1994**, *69*, 59.
(55) Richerson, D. W. *Modern Ceramic Engineering*, 2nd ed.; Marcel Dekker: New York, 1992; p 731.
(56) Gummow, R. J.; Liles, D. C.; Thackeray, M. M. *Mater. Res. Bull.* **1993**, *28*, 1249; Gummow, R. J.; Thackeray, M. M. *J. Electrochem. Soc.* **1994**, *141*, 1178; Croguennec, L.; Deniard, P.; Brec, R.; Biesan, P.; Broussely, M. *Solid State Ionics* **1996**, *89*, 127.
(57) Thackeray, M. M.; Mansuetto, M. F.; Dees, D. W.; Vissers, D. R. *Mater. Res. Bull.* **1996**, *31*, 133; Gao, Y.; Dahn, J. R. *J. Electrochem. Soc.* **1996**, *143*, 1783; Takada, T.; Hayakawa, H.; Akiba, E. *J. Solid State Chem.* **1995**, *115*, 420.
(58) Thackeray, M. M.; Mansuetto, M. F.; Johnson, C. S. *J. Solid State Chem.* **1996**, *125*, 274.
(59) Kim, J.; Manthiram, A. *J. Electrochem. Soc.* **1998**, *145*, L53.
(60) Ohzuku, T.; Kitagawa, M.; Sawai, K.; Hirai, T. *J. Electrochem. Soc.* **1991**, *138*, 360.
(61) Garcia, B.; Barboux, P.; Robot, F.; Kahn-Harari, A.; Mazerolles, L.; Baffier, N. *Solid State Ionics* **1995**, *80*, 111.
(62) Zhecheva, E.; Stoyanova, R. *Solid State Ionics* **1993**, *66*, 143.
(63) Stoyanova, R.; Zhecheva, E.; Friebel, C. *Solid State Ionics* **1994**, *73*, 1.
(64) Stoyanova, R.; Zhecheva, E. *J. Solid State Chem.* **1994**, *108*, 211; Zhecheva, E.; Stoyanova, R. *J. Solid State Chem.* **1994**, *109*, 47.
(65) Amatucci, G. G.; Tarascon, J. M.; Larcher, D.; Klein, L. C. *Solid State Ionics* **1996**, *84*, 169; Larcher, D.; Palacin, M. R.; Amatucci, G. G.; Tarascon, J. M. *J. Electrochem. Soc.* **1997**, *144*, 408; Palacin, M. R.; Larcher, D.; Audemer, A.; Sac-Epee, N.; Amatucci, G. G.; Tarascon, J. M. *J. Electrochem. Soc.* **1997**, *144*, 4226.
(66) Chiang, Y.; Young-Il, J.; Wang, H.; Huang, B.; Sadoway, D. R.; Ye, P. *J. Electrochem. Soc.* **1998**, *145*, 887.
(67) Kim, J.; Fulmer, P.; Manthiram, A. *Mater. Res. Bull.* In press.
(68) Ado, K.; Tabuchi, M.; Kobayashi, H.; Kageyama, H.; Nakamura, O.; Inaba, Y.; Kanno, R.; Takagi, M.; Takeda, Y. *J. Electrochem. Soc.* **1997**, *144*, L177.
(69) Reimers, J. N.; Rossen, E.; Jones, C. D.; Dahn, J. R. *Solid State Ionics* **1993**, *61*, 335.
(70) Kanno, R.; Shirane, T.; Kawamoto, Y.; Takeda, Y.; Takano, M.; Ohashi, M.; Yamaguchi, Y. *J. Electrochem. Soc.* **1996**, *143*, 2435.
(71) de Picciotto, L. A.; Thackeray, M. M.; David, W. I. F.; Bruce, P. G.; Goodenough, J. B. *Mater. Res. Bull.* **1984**, *19*, 1497; Manthiram, A.; Goodenough, J. B. *Can. J. Phys.* **1987**, *65*, 1309.
(72) Wilhelmi, K.; Waltersson, K.; Kihlborg, L. *Acta Chem. Scand.* **1971**, *25*, 2675; Theobald, F.; Cabala, R.; Bernard, J. *J. Solid State Chem.* **1976**, *17*, 431.
(73) Christian, P. A.; Di Salvo, F. J.; Murphy, D. W. U.S. Patent 4228226, 1980; Murphy, D. W.; Christian, P. A.; Carides, J. N. *J. Electrochem. Soc.* **1979**, *126*, 497.
(74) Manthiram, A.; Dananjay, A.; Zhu, Y. *Chem. Mater.* **1994**, *6*, 1601.
(75) Schlesinger, H. I.; Brown, H. C.; Finholt, A. E.; Gilbreath, J. R.; Hoekstra, H. R.; Hyde, E. K. *J. Am. Chem. Soc.* **1953**, *75*, 215.
(76) Tsang, C.; Kim, J.; Manthiram, A. *J. Mater. Chem.* **1998**, *8*, 425.
(77) Kim, J.; Manthiram, A. *J. Electrochem. Soc.* **1997**, *144*, 3077.
(78) Tsang, C.; Kim, J.; Manthiram, A. *J. Solid State Chem.* **1998**, *137*, 28.
(79) Tsang, C.; Dananjay, A.; Kim, J.; Manthiram, A. *Inorg. Chem.* **1996**, *35*, 504; Tsang, C.; Manthiram, A. *J. Mater. Chem.* **1997**, *7*, 1003.
(80) Tsang, C.; Lai, S. Y.; Manthiram, A. *Inorg. Chem.* **1997**, *36*, 2206.
(81) Emeleus, H. J.; Sharpe, A. G. *Modern Aspects of Inorganic Chemistry*, John Wiley & Sons: New York, 1973; p 276.
(82) Tsang, C.; Manthiram, A. *J. Electrochem. Soc.* **1997**, *144*, 520.
(83) Dahn, J. R.; Buuren, T. V.; von Sacken, U. U.S. Patent 4965150, 1990; Abraham, K. M.; Goldman, J. L.; Dempsey, D. *J. Electrochem. Soc.* **1981**, *128*, 2493; Murphy, D. W.; Christian, P. A.; Di Salvo, F. J.; Carides, J. N.; Waszczak, J. V. *J. Electrochem. Soc.* **1981**, *128*, 2053.
(84) Li, W.; Dahn, J. R.; Wainwright, D. S. *Science* **1994**, *264*, 1115.
(85) Chirayil, T. A.; Zavalij, P. Y.; Whittingham, M. S. *J. Electrochem. Soc.* **1996**, *143*, L194.
(86) Lampe-Onnerud, C.; Thomas, J. O.; Hardgrave, M.; Yde-Andersen, S. *J. Electrochem. Soc.* **1995**, 142, 3648; Bergstrom, O.; Gustafsson, T.; Thomas, J. O. *Acta Crystallogr.* **1997**, *C53*, 528.
(87) Le, D. B.; Passerini, S.; Chu, X.; Chang, D.; Owens, B. B.; Smyrl, W. H. *Rechargeable Lithium and Lithium Ion Batteries*; Megahed, S., Ed.; The Electrochemical Society Proceedings Series 94−28; The Electrochemical Society: Pennington, NJ, 1995; p 306.
(88) Tipton, A. L.; Passerini, S.; Owens, B. B.; Smyrl, W. H. *J. Electrochem. Soc.* **1996**, *143*, 3473.
(89) Hibino, M.; Ugaji, M.; Kishimoto, A.; Kudo, T. *Solid State Ionics* **1995**, *79*, 239.
(90) West, K.; Zachau-Christiansen, B.; Skaarup, S.; Saidi, Y.; Barker, J.; Olsen, I. I.; Pynenburg, R.; Koksbang, R. *J. Electrochem. Soc.* **1996**, *143*, 820.
(91) Kumagai, N.; Yu, A. *J. Electrochem. Soc.* **1997**, *144*, 830.
(92) Denis, S.; Baudrin, E.; Touboul, M.; Tarascon, J. M. *J. Electrochem. Soc.* **1997**, *144*, 4099.
(93) Besenhard, J. O.; Schollhorn, R. *J. Electrochem. Soc.* **1977**, *124*, 968; Takeda, Y.; Kanno, R.; Oyabe, Y.; Yamamoto, O. *J. Power Sources* **1985**, *14*, 215; Koksbang, R.; Norby, P. *Electrochim. Acta* **1991**, *36*, 127; Jacubec, I.; Vondrak, J.; Bludska, J. *J. Power Sources* **1992**, *39*, 133.
(94) Takeda, Y.; Kanno, R.; Tsuji, Y.; Yamamoto, O. *J. Power Sources* **1983**, *9*, 325.
(95) Yamamoto, O.; Takeda, Y.; Kanno, R.; Oyabe, Y.; Shinya, Y. *J. Power Sources* **1987**, *20*, 151.
(96) Wilhelmi, K. A. *Acta Chem. Scand.* **1968**, *22*, 2565.
(97) Murphy, D. W.; Cava, R. J.; Zahurak, S. M.; Santoro, A. *Solid State Ionics* **1983**, *9* & 10, 413.
(98) Kavan, L.; Gratzel, M.; Rathousky, J.; A. Zukal, A. *J. Electrochem. Soc.* **1996**, *143*, 394.
(99) Yagi, Y.; Hibino, M.; Kudo, T. *J. Electrochem. Soc.* **1997**, *144*, 4208.
(100) Manthiram, A.; Tsang, C. *J. Electrochem. Soc.* **1996**, *143*, L143.
(101) Wang, D.; Wen, S.; Chen, J.; Zhang, S.; Li, F. *Phys. Rev.* **1994**, *B49*, 14282.
(102) Liu, W.; Huang, X.; Wang, Z.; Li, H. Chen, L. *J. Electrochem. Soc.* **1998**, *145*, 59.
(103) Courtney, I. A.; Dahn, J. R. *J. Electrochem. Soc.* **1997**, *144*, 2045.
(104) Li, W.; Curie, J. *J. Electrochem. Soc.* **1997**, *144*, 2773.

CM980241U